
Data-induced multiscale losses and efficient multirate gradient descent schemes

Juncai He¹ Liangchen Liu² Richard Tsai^{2,3}

Abstract

This paper investigates the impact of multiscale data on machine learning algorithms, particularly in the context of deep learning. A dataset is multiscale if its distribution shows large variations in scale across different directions. This paper reveals multiscale structures in the loss landscape, including its gradients and Hessians inherited from the data. Correspondingly, it introduces a novel gradient descent approach, drawing inspiration from multiscale algorithms used in scientific computing. This approach seeks to transcend empirical learning rate selection, offering a more systematic, data-informed strategy to enhance training efficiency, especially in the later stages.

1. Introduction

In many supervised learning setups, the input data are commonly embedded in high-dimensional Euclidean spaces for convenience. To clarify, we are referring to the non-label part of the datasets (i.e. the features). A natural question arises concerning the distributions of the training data in the embedding space and their potential consequences on the efficacy of learning. A substantial body of literature (Niyogi et al., 2008; Peyré, 2009; Carlsson, 2009) has delved into the “manifold hypothesis”, which suggests the data distributions behind the complex representations might concentrate near a simpler, lower-dimensional manifold. Empirical validations (Schölkopf et al., 1998; Brand, 2002; Saul & Roweis, 2003) and the development of the theoretical testing framework (Narayanan & Mitter, 2010; Fefferman et al., 2016) have lent support to such hypothesis, and recent research (Medina et al., 2019; Brown et al., 2022) has explored its variants.

The manifold hypothesis has sparked exciting works and numerous insights discovered by the manifold learning community (Roweis & Saul, 2000; Tenenbaum et al., 2000; Belkin & Niyogi, 2003; Donoho & Grimes, 2003; Weinberger & Saul, 2006). More recently, it has found applications in the realm of deep learning in various areas, including approximation theory (Chen et al., 2019; Cloninger & Klock, 2021; Schonsheck et al., 2022), intrinsic dimensions (Brahma et al., 2015; Ansuini et al., 2019; Pope et al., 2021), initialization (Tiwari & Konidaris, 2022), and the effects of training (He et al., 2023).

Nevertheless, the predominant techniques and analysis in deep learning implicitly assume the distribution of features is full-dimensional in the embedding space and that it has the same scale across different directions. This assumption is evident in the prevalent initialization methods (Glorot & Bengio, 2010; He et al., 2015) for parameters, including those acting on the input data.

However, even under the simplistic model of principal component analysis (PCA) (Pearson, 1901; Hotelling, 1933), many real-world datasets exhibit a fast-decay spectrum in their principal directions, suggesting data distributions across different directions can manifest drastically different scales. We refer to datasets with variations in the orders of magnitude of scales across different principal directions as *multiscale datasets*, prompting a pertinent question: How do multiscale datasets impact algorithms, particularly those heavily reliant on data, such as gradient descent (GD) in deep learning? This article aims to unveil the potential impacts of multiscale data on machine learning algorithms, with a specific focus on deep learning problems. Notably, the multiscale nature of data passes down to the learning problem, giving rise to a multiscale loss landscape from various perspectives.

¹Computer, Electrical and Mathematical Science and Engineering Division, King Abdullah University of Science and Technology, Thuwal, Saudi Arabia ²Department of Mathematics, University of Texas at Austin, Austin, TX, USA ³Oden Institute for Computational Engineering and Sciences, University of Texas at Austin, Austin, TX, USA..

Stochastic gradient descent (SGD) algorithms with varying learning rates (Robbins & Monro, 1951; You et al., 2019; Smith & Topin, 2019; Liu et al., 2020) have been instrumental in the success of deep learning tasks. While it is widely believed that adopting specific learning rate schedules can significantly enhance the generalization ability of deep neural networks (DNNs), such learning rate schemes have primarily relied on empirical evidence and arguments. This suggests that there is still room for further understanding and improvement of SGD-based algorithms when applied to real-world multiscale datasets.

In the scientific computing community, multiscale algorithms such as (Engquist & Tsai, 2005; Tao et al., 2010) can efficiently compute dynamical systems where they leverage the fast averaging and near independence in components due to the gap in two widely separated scales in the systems. Drawing inspiration from these concepts, we propose a novel yet simple explicit gradient descent scheme that adopts learning rates based on multiscale information from the data. The objective is to bridge the gap between the empirical nature of learning rate choices and a more systematic, multiscale approach, ultimately aiming for the efficiency and adaptability of training algorithms for models defined on real-world multiscale datasets. While our focus doesn't extend to addressing SGD's selection of minima, we argue that the proposed algorithm is suitable for accelerating the later/final stages of gradient-based training of DNNs.

Our main contributions include:

1. We prove that multiscale data and ℓ^2 loss lead to multiscale landscapes. Specifically, we derive a multiscale expansion of the loss gradients and reveal component-wise multiscale characteristics within gradients and Hessians. We verify these theoretical findings by numerically investigating DNN models on the CIFAR dataset.
2. We propose an explicit multirate gradient descent (MrGD) scheme that leverages multiscale information to construct an appropriate learning rate schedule for much-enhanced convergence speed.
3. We establish a comprehensive and rigorous theory demonstrating that the MrGD scheme achieves a quasi-optimal convergence rate for linear problems and can be extended to convex functions.

1.1. Related Work

Multiscale landscape of loss in learning. There has been considerable discussion about the origins of the multiscale expansion form in the loss gradient. (Mei et al., 2018) suggests a possible origin of the loss with a multiscale structure arising from the effect of noise in various statistical models. (Kong & Tao, 2020) demonstrates that a simple 2-layer neural network (NN) using a periodic activation function trained with multiscale data leads to a loss exhibiting a multiscale expansion. They also show that deterministic gradient descent can become stochastic with a sufficiently large learning rate. (Ma et al., 2022) numerically observe a multiscale behavior in the loss landscape of neural network loss functions, which is manifested in two ways: (1) in the vicinity of minima, the loss combines a continuum of scales and grows sub-quadratically, and (2) over a larger region, the loss displays several distinct scales. Recently, (He et al., 2023) analyzed linear regression on two-scale data sampled from a distribution that concentrates around a lower dimensional linear subspace. The regression solutions reflect scales corresponding to the underlying data. Their results also reveal a non-trivial relationship between the number of data points and the magnitude of the smaller scale, which is crucial for the stability of the linear model, a concept that extends to deep neural networks. (Liu et al., 2023) extended the data distributions to embedded curved manifolds, providing closed-form solutions for local linear regression on hypersurfaces and curves, indicating a potential influence of the multiscale geometric properties of the underlying data manifold on the regression solutions.

Larger learning rates in GD and SGD Several studies, both numerical (Loshchilov & Hutter, 2017; You et al., 2019; Smith & Topin, 2019; Liu et al., 2020) and theoretical (Oymak, 2021; Wang & Yuan, 2023; Das Gupta et al., 2023; Grimmer, 2023), have shown that an appropriately larger learning rate can benefit the training of GD and SGD in general convex optimization and deep learning. However, most of these studies focus on improvements for better generalization, such as Warm Restart (Loshchilov & Hutter, 2017) for training general NNs towards flat local minima (He et al., 2019), or for specific problems like matrix factorization (Wang et al., 2022) and deterministic and stochastic Hamiltonian dynamical systems (Li et al., 2023). In this work, we propose a multiscale landscape perspective of the empirical loss and demonstrate that appropriately larger learning rates may also contribute to improved convergence during training.

2. The loss landscape

In this section, we discuss the empirical loss landscape arising from multiscale data. We first make a key assumption on the data in the following:

Assumption 2.1. The dataset, $\{(\mathbf{x}_i, g(\mathbf{x}_i))\}_{i=1}^N \subset \mathbb{R}^{d+1}$, comprises N *i.i.d.* samples $\{\mathbf{x}_i\}_{i=1}^N \subset \mathbb{R}^d$ drawn from distributions with a *component-wise multiscale structure*. This structure signifies the distribution scales along different directions can be organized into $(m + 1)$ groups based on their magnitude, where $\sum_{i=0}^m d_i = d$. More specifically, there exists a unitary matrix $UU^T = I_{d \times d}$ s.t.

$$\tilde{\mathbf{x}}_i = U^T(\mathbf{x}_i - \bar{\mathbf{x}}), \quad (1)$$

where $\tilde{\mathbf{x}}_i$ satisfies:

$$\tilde{\mathbf{x}}_i = (\tilde{\mathbf{x}}_i^0, \varepsilon_1 \tilde{\mathbf{x}}_i^1, \dots, \varepsilon_m \tilde{\mathbf{x}}_i^m)^T \in \mathbb{R}^d, \quad (2)$$

with $1 \gg \varepsilon_1 \gg \varepsilon_2 \gg \dots \gg \varepsilon_m > 0$. Here, $\mathbf{x}_i^k \sim \mathcal{U}_k$ on \mathbb{R}^{d_k} for $k = 0 : m$, each representing a group of directions of the k^{th} -scale, where \mathcal{U}_k is the corresponding uniform distribution with a scale of $\mathcal{O}(1)$ in all directions.

In practice, PCA can be used to transform data into the above form. Thus, for the convenience of analysis, we shall assume the presence of such preprocessing and identify $\tilde{\mathbf{x}}_i$ with \mathbf{x}_i , i.e. $U = I$ and $\bar{\mathbf{x}} = \bar{\mathbf{0}}$.

2.1. Logistic regression with multiscale data

We consider logistic regression for classifying the input vector \mathbf{x} into k -classes, with a learning function $f(\mathbf{x}; W) : \mathbb{R}^d \mapsto \mathbb{R}^k$,

$$[f(\mathbf{x}; \mathbf{w}, b)]_j = \frac{e^{\mathbf{w}_j \cdot \mathbf{x} + b_j}}{\sum_{i=1}^k e^{\mathbf{w}_i \cdot \mathbf{x} + b_i}}, \quad j = 1 : k, \quad (3)$$

and the cross-entropy loss

$$\mathcal{L}_c(W) = -\frac{1}{N} \sum_{i=1}^N g(\mathbf{x}_i) \cdot \log f(\mathbf{x}_i; W). \quad (4)$$

The subsequent proposition illustrates the emergence of multiscale gradient components due to multiscale data:

Proposition 2.2. *When the data $\{\mathbf{x}_i\}_{i=1}^N$ satisfies Assumption 2.1, the loss in (4) has a multiscale gradient component:*

$$\frac{\partial \mathcal{L}_c}{\partial \mathbf{w}} \sim (\mathcal{O}(1), \mathcal{O}(\varepsilon_1), \mathcal{O}(\varepsilon_2) \dots), \quad (5)$$

where $\mathcal{O}(\varepsilon_j)$ is a group of vectors in \mathbb{R}^k of magnitudes bounded above by a constant multiple of ε_j .

Proof. See Appendix C.1. □

We remark that an identical form of the gradient also arises in linear regression problem with the least square loss.

2.2. Deep learning with multiscale data

We consider neural network function classes defined by

$$\begin{cases} f^0(\mathbf{x}) & = \mathbf{x} \\ f^\ell(\mathbf{x}; W) & = \sigma(W^\ell f^{\ell-1}(\mathbf{x}) + b^\ell), \quad \ell = 1 : L, \\ f(\mathbf{x}; W) & = W^{L+1} f^L(\mathbf{x}) \end{cases} \quad (6)$$

where σ is the activation function. The entries in the matrix W^ℓ will be denoted by $W_{i,j}^\ell$. We will use the simple least square loss

$$\mathcal{L}(W) = \frac{1}{2N} \sum_{i=1}^N (f(\mathbf{x}_i; W) - g_i)^2. \quad (7)$$

Multiscale gradient components Due to the multiplicative structure in the network’s first layer, the neural networks defined in (6) can be represented as $f(x, W) = \tilde{f}(W^1 x; W^2)$. This form is reminiscent of those from the regression models (3), indicating a comparable multiscale effect on W_1 , similar to Proposition 2.2.

Proposition 2.3. *Suppose $f^1 \in \mathbb{R}^{n_1}$. When the data $\{\mathbf{x}_i\}_{i=1}^N$ satisfies Assumption 2.1, the loss (7) has:*

$$\frac{\partial \mathcal{L}}{\partial W_{i,:}^1} \sim (\mathcal{O}(1), \mathcal{O}(\varepsilon_1), \mathcal{O}(\varepsilon_2) \dots), \quad 1 \leq i \leq n_1, \quad (8)$$

where $\mathcal{O}(\varepsilon_i)$ are components in the gradient of order ε_i .

Proof. See Appendix C.2. □

We conduct the following experiments to verify the proposition empirically. We train a simple 3-layer multi-layer perceptron (MLP) of sizes 3072-1024-128-10 using full gradient descent with the cross-entropy loss on the CIFAR10 dataset (Krizhevsky et al., 2009). The dataset is pre-aligned using PCA, as described in Assumption 2.1. We examine the magnitude of $\partial \mathcal{L} / \partial W_{i,:}^1$ for $i = 1$ and another randomly chosen index. Figure 1 shows these quantities at different stages of training, corresponding to test accuracies around 30% and 50%. (Trained 3-layer MLPs typically reach a test accuracy cap of around 60% for CIFAR.) We then compare the gradients across the first and second hidden layers.

From Figure 1, it is evident that the raw gradient magnitudes of the first hidden layer closely track the decay of the scale of the data distribution. In contrast, the gradient in the second hidden layer exhibits a more uniformly scattered pattern. This reconfirms the fact that the gradient in the first layer is primarily characterized by the data.

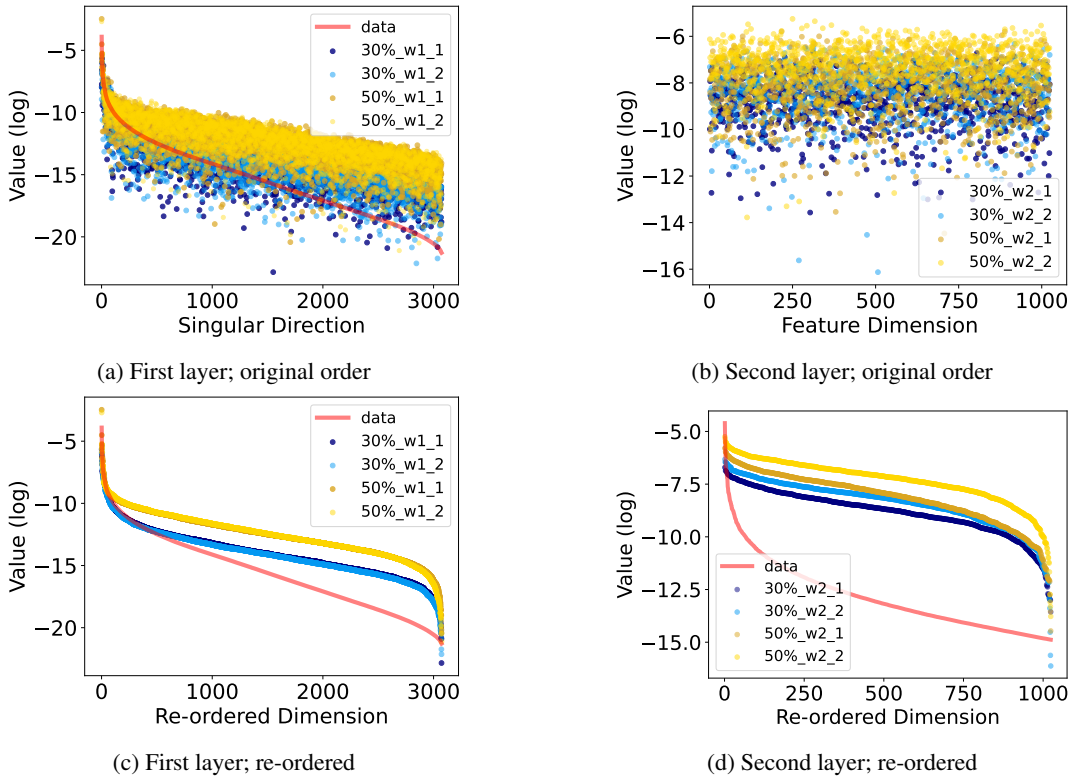


Figure 1. The magnitudes of the loss gradient with respect to $W_{1,:}^1$ and $W_{i,:}^1$ for a randomly chosen $i > 0$ on the natural log scale; the quantities are labelled w_{1_1} and w_{1_2} respectively. Two models with test accuracy 30% (blue) and 50% (yellow) are investigated. The bottom row has gradient values sorted by their magnitudes. The red curve represents the principal values of the training data, scaled to align with the gradient magnitude for better comparison. The red curve is truncated in the bottom-right.

If the data exhibits a power cascade of scales, one can further derive a multiscale expansion of the loss gradient with respect to *all* weights in the network.

Multiscale expansion of the loss gradient We consider a special case of (2), in which

$$\mathbf{x}_i = (\mathbf{x}_i^0, \varepsilon \mathbf{x}_i^1, \varepsilon^2 \mathbf{x}_i^2, \dots, \varepsilon^m \mathbf{x}_i^m)^T, \quad (9)$$

for some $\varepsilon \ll 1$. We establish in the following Theorem:

Theorem 2.4. *For any functions defined in (6), the loss function (7) with a dataset under Assumption 2.1 along with (9):*

$$\frac{\partial \mathcal{L}}{\partial W^\ell} = \frac{1}{N} \sum_{k=0}^m \varepsilon^k A_k^\ell(\mathbf{x}^0, \dots, \mathbf{x}^k), \quad (10)$$

$$A_0^\ell(\mathbf{x}^0) = (f(\mathbf{x}^0) - g(\mathbf{x}^0)) \tilde{\lambda}^\ell(\mathbf{x}^0) (f^{\ell-1}(\mathbf{x}^0))^T, \quad (11)$$

where $\tilde{\lambda}^\ell(\mathbf{x}^0)$ is a tensor product related to $\partial f / \partial f^\ell$, given in Equation (50), and $A_k^\ell(\mathbf{x}^0, \dots, \mathbf{x}^k)$ is of $\mathcal{O}(1)$ defined in Equation (115).

Proof. Apply induction on each component of the loss gradient. For details, see Appendix B. \square

Notice that in the power series, A_k^ℓ depends *only* on the first $k + 1$ coordinates. Therefore, the empirical loss is relatively insensitive to the smaller scale coordinates, $\mathbf{x}^\nu, \nu = 2, 3, \dots$. Consequently, relying solely on monitoring the training loss may not provide a sufficiently accurate indication of the inference quality, especially for inputs close to the tail of the multiscale data distribution.

With such an additive multiscale structure of the loss gradient, (Kong & Tao, 2020) show that solutions of the deterministic GD may exhibit stochastic behavior. However, this observation is contingent upon an assumption that the small scales are periodic in a weak sense. Analyzing the loss gradient with all scales mixed up is, in general, challenging and beyond the scope of this work.

Multiscale Hessian A multitude of studies have utilized local quadratic approximations and second-order information of the loss to scrutinize the training dynamics of deep neural networks (Wu et al., 2018; Du et al., 2018; Jacot et al., 2018). In these investigation, the convergence behavior of the neural network and the selection of minima are typically influenced by the eigenvalues of the Hessian. On the other hand, of particular concern to us is the learning rate schedule for the gradient-based training of neural networks. Inevitably, the learning rate is limited by the stability of the SGD, a constraint determined by the eigenvalues of the loss's Hessian. Thus, the characteristics of the Hessian play a crucial role in unraveling many underlying issues.

Following the previous derivation, we present a result demonstrating the connections between the data's characteristics and the Hessian of the weights related to the first layer, denoted by $\nabla_{W_{i,:}^1}^2$:

Proposition 2.5. *Let $f^1 \in \mathbb{R}^{n_1}$. Then for any $1 \leq i \leq n_1$*

$$\nabla_{W_{i,:}^1}^2 \mathcal{L} = \frac{1}{2N} \sum_{j=1}^N s_i(\mathbf{x}_j) \mathbf{x}_j \mathbf{x}_j^T \approx \left(\sum_{j=1}^N s_i(\mathbf{x}_j) \right) X^T X,$$

where, denoting the first argument of \tilde{f} as $\mathbf{z} = (z_1, z_2, \dots, z_{n_1})$,

$$s_i(\mathbf{x}_j) := c_i(\mathbf{x}_j)^2 + (f(\mathbf{x}_j, W) - g_j) \frac{\partial^2 \tilde{f}(\mathbf{z}, W^2)}{\partial z_i^2} \in \mathbb{R}, (W_{i,:}^1 \mathbf{x}_j)^2 \in \mathbb{R}. \quad c_i(\mathbf{x}_j) := \frac{\partial \tilde{f}(\mathbf{z}, W^2)}{\partial z_i} \in \mathbb{R}$$

for $\mathbf{z} = W^1 \mathbf{x}_j$.

Proof. See Appendix C.3. \square

Note $X^T X$ is the (sample) covariance matrix. Therefore, the spectral distribution of the Hessian $\nabla_{W_{i,:}^1}^2 \mathcal{L}$ at any stage of training should also resemble that of the data, up to a constant multiplier. The same analysis applies to $\nabla_{W_{s,:}^1} \nabla_{W_{t,:}^1} \mathcal{L}$ for any $1 \leq s, t \leq n_1$.

We also confirm this observation through the same numerical experiments setups as before, and present the results in Figure 2. We notice that, at any stage of training, the spectrum of the Hessian for the first layer displays a decay trend identical to the spectrum of the data. Notably, the spectrum of the Hessian for the second layer also demonstrates a rapid decay in its leading components. We conjecture this phenomenon is related to Theorem 2.4. This phenomenon is also evident in the training of MNIST (refer to Figure 4).

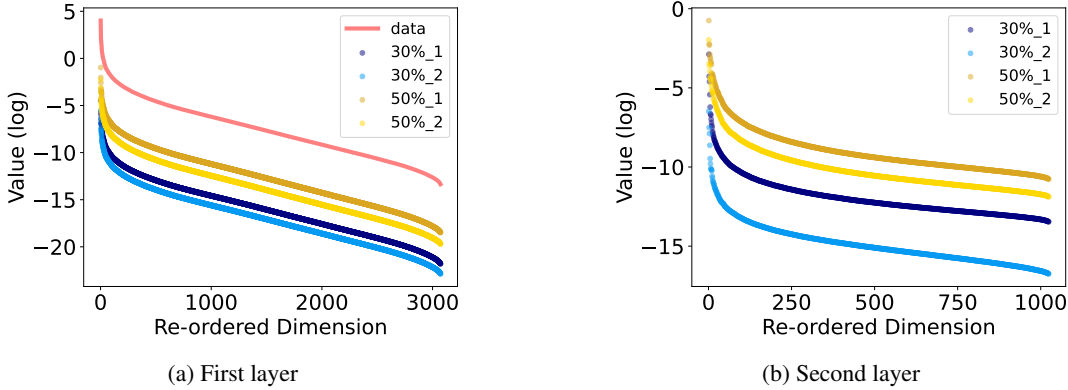


Figure 2. Eigenvalues of the Hessians, $\nabla_{W_{i,:}^1}^2 \mathcal{L}$ and $\nabla_{W_{i,:}^2}^2 \mathcal{L}$, on the natural log scale, under the same setup as in Figure 1. The eigenvalues are sorted by magnitude. The original eigenvalues (not shown) only exhibit slight jittering toward the ending dimensions, with overall trends closely mirroring the ordered ones.

Extending a parallel derivation to previous regression models also leads to a Hessian characterized by the data covariance matrix, due to the structural resemblance between these models. The above observations bring forth the question: how can one leverage such information to devise gradient descent algorithms that effectively exploit the inherent multiscale characteristics identified in the data?

3. Multirate gradient descent

In this section, we introduce and analyze a novel gradient descent algorithm, tailored for the cases discussed in the previous section. It will become evident that by a blend of large and small learning rates, the algorithm capitalizes on the multiscale characteristics, resulting in accelerated convergence.

3.1. Multirate gradient descent for quadratic problems

Consider the following minimization problem:

$$\min_{\theta \in \mathbb{R}^d} \mathcal{L}(\theta) := \frac{1}{2} \theta^T A \theta - g^T \theta, \quad (12)$$

where A is a $d \times d$ symmetric matrix with strictly positive eigenvalues, and the eigenvalues can be divided into m groups, each comprising d_i members such that $d = \sum_i^m d_i$, following Assumption 2.1 for data. These eigenvalues are arranged in non-increasing order as:

$$\sigma_{1,1} \geq \sigma_{1,2} \geq \dots \geq \sigma_{1,d_1} > \sigma_{2,1} \geq \dots \geq \sigma_{2,d_2} > \dots > \sigma_{m,1} \geq \dots \geq \sigma_{m,d_m} \quad (13)$$

For $i = 1 : m$, denote $\sigma_i := \sigma_{i,1}$ the principal eigenvalue and $\kappa_i := \frac{\sigma_{i,1}}{\sigma_{i,d_i}}$ the local condition number for group i . Additionally, we introduce the definition of decay rate:

Definition 3.1. The *decay rate* between consecutive groups of eigenvalues is defined by:

$$r_i := \frac{\sigma_{i+1}}{\sigma_i} = \frac{\sigma_{i+1,1}}{\sigma_{i,1}} \text{ for } i = 1 : m - 1.$$

We consider the case $r_i \leq r \ll 1$ for $i = 1 : m - 1$, and propose an explicit gradient descent scheme involving multiple learning rates η_i for $i = 1 : m$. The algorithm is defined in Algorithm 1.

Algorithm 1 Multirate Gradient Descent (MrGD)

1: **Input:**

- θ^0 : the initial guess (typically zeros or random);
- η_i : the learning rate on the i -th scale;
- n_i : the number of iterations on the i -th scale;
- K : the number of outer iterations.

2: **for** $k = 1 : K$ **do**

3:

$$\theta_{m,0}^k := \theta^{k-1}$$

4: **for** $i = m : -1 : 1$ **do**

5: **for** $l = 1 : n_i$ **do**

6:

$$\theta_{i,l}^k := \theta_{i,l-1}^k - \eta_i \nabla \mathcal{L}(\theta_{i,l-1}^k) \quad (14)$$

7: **end for**

8:

$$\theta_{i-1,0}^k := \theta_{i,n_i}^k$$

9: **end for**

10:

$$\theta^k := \theta_{1,n_1}^k$$

11: **end for**

12: **Output:** θ^K

To analyze the convergence property of Algorithm 1, we investigate the error dynamics:

Let θ^* be the global minimum, which satisfies the optimality condition $A\theta^* = g$, and $e_{j,l}^k := \theta_{j,l}^k - \theta^*$ be the error at each step where i is replaced by j for clarity in subsequent discussion. Then, based on Equation (14), we have $e_{j,l}^k = e_{j,l-1}^k - \eta_j A e_{j,l-1}^k$. Therefore, the error propagation operator S for one outer iteration can be written as

$$S = Q_1^{n_1} Q_2^{n_2} \cdots Q_{m-1}^{n_{m-1}} Q_m^{n_m}, \quad (15)$$

where

$$Q_j = I - \eta_j \nabla^2 \mathcal{L} = I - \eta_j A, \text{ for } j = 1 : m. \quad (16)$$

Given the gaps between different groups of eigenvalues as depicted in 13, for each iteration with Q_j , we select learning rates ensuring the reduction of components of θ in the j -th eigenspace. Specifically, we choose

$$\eta_j \sim \mathcal{O}\left(\frac{1}{\sigma_j}\right), \text{ with } \eta_j \leq \frac{1}{\sigma_j}, \quad (17)$$

or we express it as $\eta_j \lesssim \mathcal{O}(1/\sigma_j)$. Notably, Equation (17) results in a periodic learning rate scheme in Algorithm 1, with monotonicity maintained within each of the K outer iterations. Remark 3.6 provides further discussion on η_j .

The learning rates in Equation (17) also leads to uniform convergence in the i -th eigenspace with any $i \geq j$, with the convergence rate being linked to the smallest eigenvalue in the i -th group: σ_{i,d_i} as outlined in the following remark:

Remark 3.2. For $j \leq i$, where $i, j = 1 : m$, since $\eta_j \sigma_{i,d_i} \lesssim \sigma_{i,d_i} / \mathcal{O}(\sigma_j) \leq 1$, the convergence rate for Q_j , when the parameter θ is restricted to the eigenspace V_i associated with $\{\sigma_{i,1}, \dots, \sigma_{i,d_i}\}$, is determined by η_j and σ_{i,d_i} , s.t.

$$\sup_{v_i \in V_i, \|v_i\|=1} \|Q_j v_i\| \leq (1 - \eta_j \sigma_{i,d_i}) = (1 - R_i^j \kappa_i^{-1}),$$

where in the last equality, we denote $R_i^j := \eta_j \sigma_i$ for demonstrating the role of the local condition number κ_i . For $j > i$, $\sigma_i \gg \sigma_j \implies \eta_j \sigma_i \gg 1$, implying θ restricted to V_i will be growing, where the growth is related to $|1 - \eta_j \sigma_i| = |1 - R_i^j| \gg 1$.

Remark 3.3. For the convenient of further analysis and better readability, we summarize for R_i^j that the relative magnitude of j and i determines if θ is convergent or growing in the eigenspace V_i under the learning rate η_j . Specifically, θ restricted to V_i is:

$$\begin{cases} \text{growing with rate } \sim \mathcal{O}(|1 - R_i^j|) \gg 1, & \text{if } j > i \text{ in } R_i^j \\ \text{convergent with rate } \leq (1 - R_i^j \kappa_i^{-1}), & \text{if } j \leq i \text{ in } R_i^j \end{cases}$$

By showing $\|S\| \leq 1$, the following theorem indicates Algorithm 1 is uniformly convergent, provided the inner iteration numbers n_1, n_2, \dots, n_{m-1} are chosen appropriately, with $n_m = 1$, which will be justified later.

Theorem 3.4. For $n_m = 1$ and any $n_{m-1}, n_{m-2}, \dots, n_1$ satisfying

$$n_i \geq \left\lceil \sum_{j=i+1}^m n_j F_{i,j} \right\rceil, \quad (18)$$

where $F_{i,i+1} =$

$$\left(-\log(r_i) + \log \left(\frac{|r_i - R_{i+1}^{i+1}|}{1 - R_{i+1}^{i+1} \kappa_{i+1}^{-1}} \right) \right) / \log \left(\frac{1 - R_{i+1}^i \kappa_{i+1}^{-1}}{1 - R_i^i \kappa_i^{-1}} \right)$$

and $F_{i,j} =$

$$\left(-\log(r_i) + \log \left(\frac{|r_i - R_{i+1}^j|}{|1 - R_{i+1}^j|} \right) \right) / \log \left(\frac{1 - R_{i+1}^i \kappa_{i+1}^{-1}}{1 - R_i^i \kappa_i^{-1}} \right)$$

for all $j = i + 2 : m$ and $R_i^i := \eta_i \sigma_i$, we have

$$\|S\| \leq \prod_{j=1}^m (1 - R_m^j \kappa_m^{-1})^{n_j}. \quad (19)$$

Proof. See Appendix D.1 □

Remark 3.5. Here, we justify the choice of $n_m = 1$. One can rewrite (18) as:

$$\begin{aligned} n_{m-1} &\geq n_m F_{m-1,m}, \\ n_{m-2} &\geq n_m F_{m-2,m} + n_{m-1} F_{m-2,m-1} \\ &\geq (F_{m-2,m} + F_{m-1,m} F_{m-2,m-1}) n_m, \dots \end{aligned}$$

indicating the lower bound for any n_i scales linearly with n_m , i.e., $n_i \geq c_i n_m$ for some constants c_i 's. Therefore, for a fixed problem, the final iteration number n_m determines the rest of n_i 's.

Furthermore, using the linearity of Q_i , the error propagation operator for Algorithm 1 can be expressed as:

$$S^K = (Q_1^{n_1} Q_2^{n_2} \dots Q_{m-1}^{n_{m-1}} Q_m^{n_m})^K = Q_1^{K n_1} Q_2^{K n_2} \dots Q_{m-1}^{K n_{m-1}} Q_m^{K n_m}.$$

Therefore, for any desired value of n_m , one can simply set $n_m = 1$ in Algorithm 1 and execute the outer iterations the desired number of times. Thus, we assume $n_m = 1$ throughout the remainder.

Remark 3.6. The linearity of Q_i also guarantees that the order of iterations associated with n_i does not affect the outcome. This implies that Algorithm 1 will converge regardless of whether the learning rate scheme for η_i 's is monotonic or not, as long as η_i 's satisfy Equation (17) and the corresponding iteration number n_i 's satisfy the result presented in Theorem 3.4.

3.1.1. COMPARISON WITH TRADITIONAL METHODS

Assumption 3.7. Consider a special case where the local condition numbers and decay rates in the original system (12) are equal and relatively small, respectively, i.e.,

$$\kappa_i = \kappa_c \gtrsim \mathcal{O}(1) \quad \text{and} \quad r_i = r \ll 1. \quad (20)$$

The above assumption ensures a hierarchical structure in the eigenvalue clusters with a global condition number:

$$\kappa = \frac{\sigma_{1,1}}{\sigma_{m,d_m}} = \frac{\sigma_{1,1}}{\sigma_{2,1}} \frac{\sigma_{2,1}}{\sigma_{3,1}} \dots \frac{\sigma_{m-1,1}}{\sigma_{m,1}} \frac{\sigma_{m,1}}{\sigma_{m,d_m}} = \kappa_c r^{1-m} \gg 1.$$

In addition, following Equation (17), we set the multirate η_i 's based on some constant $\eta \gtrsim 1$, s.t.,

$$\eta_i = \frac{1}{\eta \sigma_i} \lesssim \mathcal{O}\left(\frac{1}{\sigma_i}\right).$$

Thus, for the vanilla GD with a constant learning rate η_1 , we need $\eta_1 \lesssim \mathcal{O}(\frac{1}{\sigma_1})$ to ensure convergence and the convergence rate is then given by $(1 - 1/(\kappa_c r^{1-m}))$. To achieve an error of $\mathcal{O}(\varepsilon)$:

$$\left(1 - \frac{1}{\kappa_c r^{1-m}}\right)^n < \mathcal{O}(\varepsilon) \implies n \gtrsim \mathcal{O}(\kappa_c r^{1-m} |\log(\varepsilon)|) \quad (21)$$

we need n many vanilla GD steps as indicated above. For accelerating methods, such as Conjugate Gradient (Hestenes et al., 1952), GD with momentum (Polyak, 1964), Chebyshev iterations (Manteuffel, 1977), Nesterov acceleration (Nesterov, 1983), etc., one may need

$$\mathcal{O}\left(\sqrt{\kappa_c r^{1-m} |\log(\varepsilon)|}\right). \quad (22)$$

Now, we demonstrate how MrGD can accelerate convergence by using multiple learning rates. As a direct consequence of Theorem 3.4, we have the following uniform convergence result:

Corollary 3.8. Under Assumption 3.7, Theorem 3.4 yields:

$$\|S\| \leq \prod_{j=1}^m (1 - R_m^j \kappa_m^{-1})^{n_j} \leq \left(1 - \frac{1}{\eta \kappa_c}\right). \quad (23)$$

Since $\kappa_c \gtrsim \mathcal{O}(1)$, we can also choose a constant $\eta > 1$ such that $\frac{1}{\eta \kappa_c} \lesssim \mathcal{O}(1)$. Following the same derivation as in (21), we need only $\mathcal{O}(|\log(\varepsilon)|)$ outer iterations in MrGD to achieve an error of $\mathcal{O}(\varepsilon)$. The number of total GD iterations with different learning rates is then:

$$\mathcal{O}(n |\log(\varepsilon)|), \quad (24)$$

where $n = \sum_{i=1}^m n_i$ is the number of GD iterations in one step of outer iteration.

The only question left is how n compares with $\kappa_c r^{1-m}$ under Assumption 3.7. As mentioned in Remark 3.5, the lower bound for n is characterized completely by $F_{i,j}$ for any $j \geq i + 1$. As a result, we provide upper bounds for $F_{i,j}$ below under a more general case than Assumption 3.7:

Corollary 3.9. For any fixed $0 < r \ll 1$ and $\eta \kappa_c \gtrsim \mathcal{O}(1)$, we have $F_{i,i+1}, F_{i,j} \geq 0$, and

$$\begin{cases} F_{i,i+1} \leq \frac{\eta \kappa_c (\eta \kappa_c - r) (-\log(r(\eta \kappa_c - 1)) + \kappa_c - \eta r - 1)}{\eta \kappa_c (1 - r) - r} \\ F_{i,j} \leq \frac{\eta \kappa_c (\eta \kappa_c - r) (-\log(r) + C r^{j-(i+1)})}{\eta \kappa_c (1 - r) - r}, \end{cases}$$

for $j = i + 2 : m$. This means, as $r \rightarrow 0$, we have

$$F_{i,j} = \mathcal{O}(\eta \kappa_c |\log(r)|) \quad (25)$$

for all $j = i + 1 : m$, which leads to the estimate for n :

$$n = \mathcal{O}\left((\eta \kappa_c)^{m-1} |\log(r)|^{m-1}\right). \quad (26)$$

Proof. See Appendix D.2. □

The scenario described addresses problems possessing pronounced hierarchical spectral structures in the asymptotic regime as $r \rightarrow 0$. For these problems, MrGD demonstrates significant enhancements, attaining an improvement factor of $|\log(r)|$, in contrast to the polynomial improvement factor seen within other gradient descent techniques.

Lastly, we examine a harmless scenario where $\kappa_c \gtrsim 1$ as a basic validation step. In this instance, having knowledge of the eigenvalue groups essentially equates to knowing almost all the eigenvalues. Any algorithm utilizing such information should ideally demonstrate rapid convergence. Indeed, for MrGD, for any fixed $r > 0$ and $\kappa_c \gtrsim 1$, as $\eta \rightarrow 1^+$ such that $\eta\kappa_c \rightarrow 1^+$, we have

$$F_{i,i+1} \rightarrow 1 \text{ and } F_{i,j} \rightarrow 0, \text{ for } j = i + 2 : m. \quad (27)$$

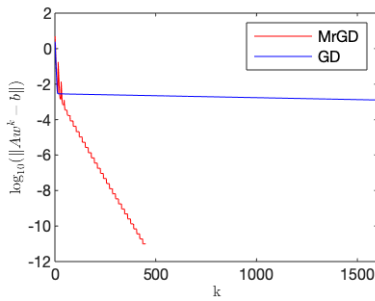
This results in $n_j \approx n_m = 1$ for all $j = 1 : m - 1$, leading to $n = \sum_{i=1}^m n_i \rightarrow m$, and an overall complexity of $\mathcal{O}(m|\log(\varepsilon)|)$ for MrGD. This aligns with our intuition as the MrGD method effectively adopts the learning rate $\frac{1}{\sigma_i}$ for the iterations associated with $n_i = 1$, resulting in a one-step convergence for group i .

Furthermore, for certain specific problems, the multigrid methods (Xu, 1992; Hackbusch, 2013) also achieve a similar rapid convergence of complexity $\mathcal{O}(m|\log(\varepsilon)|)$. However, as highlighted in (Lee et al., 2007; Xu & Zikatanov, 2017), constructing such an efficient multigrid method typically requires detailed knowledge of the operator’s eigenspace.

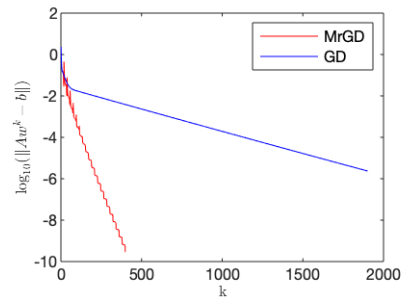
In Table 1, the methods discussed above are compared in terms of computational complexity and necessary information. Figure 3 illustrates two examples of convergence profiles for GD and MrGD on 100-dimensional linear regression problems with different number of scales.

Table 1. Comparison of time complexities required to achieve $\mathcal{O}(\varepsilon)$ -error using various methods, along with the corresponding information needed. “e.val” stands for eigenvalues, and “GD+” stands for gradient decent methods with accelerations related to (22). $\kappa_c \approx 1$ is the local condition number, and $r \ll 1$ is the decay rate of eigenvalues.

	GD	GD+	MrGD	Multigrid
Complexity	$\mathcal{O}\left(\frac{\kappa_c \log(\varepsilon) }{r^{m-1}}\right)$	$\mathcal{O}\left(\frac{\sqrt{\kappa_c} \log(\varepsilon) }{\sqrt{r^{m-1}}}\right)$	$\mathcal{O}((\eta\kappa_c \log(r))^{m-1} \log(\varepsilon))$	$\mathcal{O}(m \log(\varepsilon))$
Information	largest e.val	largest e.val	e.val clusters	eigenspace



(a) Two scales with $r = 0.001$



(b) Three scales with $r = 0.1$

Figure 3. Numerical examples for randomly generated 100-dimensional linear regression problem with two scales ($m = 1$, $r = 0.001$) and three scales ($m = 2$, $r = 0.1$). More details of this example can be found in Appendix E.

3.2. Multirate gradient descent for convex problems

In this section, we extend the insights obtained from the quadratic minimization problems (12) to more general convex minimization problems. Consider

$$\min_{\theta \in \mathbb{R}^d} \mathcal{L}(\theta),$$

for $\mathcal{L} : \mathbb{R}^d \mapsto \mathbb{R}$ L -smooth and μ -strongly convex, *i.e.*,

$$\mu \mathbf{I}_d \preceq \nabla^2 \mathcal{L}(\theta) \preceq L \mathbf{I}_d. \quad (28)$$

We introduce the following assumptions:

Assumption 3.10. There exists an orthogonal matrix $\Pi \in \mathbb{R}^{d \times d}$ of the form:

$$\Pi^T = [\Pi_1^T | \Pi_2^T | \dots | \Pi_m^T] \in \mathbb{R}^{d \times d}, \quad (29)$$

with $\Pi_i \in \mathbb{R}^{d_i \times d}$ such that

$$\sigma_{i,d_i} \mathbf{I}_{d_i} \preceq \Pi_i \nabla^2 \mathcal{L}(\theta) \Pi_i^T \preceq \sigma_{i,1} \mathbf{I}_{d_i}. \quad (30)$$

for $\sigma_{i,1}$, σ_{i,d_i} satisfying (13) for $i = 1 : m$. Furthermore, we assume the cross-spectrum is bounded by a small positive number $0 \leq \delta \ll 1$ for any $i \neq j$:

$$\|\Pi_i \nabla^2 \mathcal{L}(\theta) \Pi_j^T\| \leq \delta. \quad (31)$$

Then, the convergence result of the MrGD Algorithm 1 introduced in Theorem 3.4 can be generalized to convex problems by the following theorem:

Theorem 3.11. Let $\theta_{i,l}^k$ be computed by Algorithm 1 for minimizing (28), with iteration numbers $n_{m-1}, n_{m-2}, \dots, n_1$ satisfying (18). If $\|\theta_{i,l}^k - \theta^*\| \leq C$ for all $i = 1 : m$ and $l = 1 : n_i$, for some constant C , under Assumptions 3.10,

$$\|\theta^k - \theta^*\| \leq \prod_{j=1}^m (1 - R_m^j \kappa_m^{-1})^{n_j} \|\theta^{k-1} - \theta^*\| + \delta m C \max_{i=1:m} \left\{ \sum_{j=0}^{m-1} \eta_{j+1} C_i^j E_i^j \right\},$$

where, when $j \leq i$,

$$C_i^j = \prod_{s=1}^j (1 - R_i^s \kappa_i^{-1})^{n_s} \quad \text{and} \quad E_i^j = \sum_{s=0}^{n_j-1} (1 - R_i^j \kappa_i^{-1})^s,$$

and when $j > i$,

$$C_i^j = \prod_{s=1}^i (1 - R_i^s \kappa_i^{-1})^{n_s} \prod_{s=i+1}^j |1 - R_i^s|^{n_s} \quad \text{and} \quad E_i^j = \sum_{s=0}^{n_j-1} |1 - R_i^j|^s,$$

and $R_i^j = \eta_j \sigma_{i,1} = \eta_j \sigma_i$ as defined in Remark 3.2.

Proof. See Appendix D.3. □

The following Theorem states that if the cross-spectrum δ vanishes, we can recover results identical to Theorem 3.4:

Corollary 3.12. With assumption (31) replaced by $\|\Pi_i \nabla^2 \mathcal{L}(\theta) \Pi_j^T\| = 0$ for any $i \neq j$, and all other hypotheses in Theorem 3.11 standing,

$$\|\theta^k - \theta^*\| \leq \prod_{j=1}^m (1 - R_m^j \kappa_m^{-1})^{n_j} \|\theta^{k-1} - \theta^*\|. \quad (32)$$

Furthermore, under Assumption 3.7, we have

$$\|\theta^k - \theta^*\| \leq \left(1 - \frac{1}{\eta \kappa_c}\right) \|\theta^{k-1} - \theta^*\|. \quad (33)$$

Proof. Take $\delta = 0$ in Theorem 3.11 □

An illustrative example of the above scenario is when the loss function takes the form:

$$\mathcal{L}(\theta) = \frac{1}{2} \theta^T A \theta - g^T \theta + \sum_{i=1}^m f_i(\Pi_i \theta), \quad (34)$$

where $\Pi = [\Pi_1^T | \Pi_2^T | \dots | \Pi_m^T] \in \mathbb{R}^{d \times d}$ forms the spectral decomposition of A with $\frac{1}{2}\sigma_{i,d_i} \mathbf{I}_{d_i} \preceq \Pi_i A \Pi_i^T \preceq \frac{1}{2}\sigma_{i,1} \mathbf{I}_{d_i}$ and $f_i : \mathbb{R}^{d_i} \mapsto \mathbb{R}$ are arbitrary convex functions with $\frac{1}{2}\sigma_{i,d_i} \mathbf{I}_{d_i} \preceq \nabla^2 f_i(\theta) \preceq \frac{1}{2}\sigma_{i,1} \mathbf{I}_{d_i}$ for all $i = 1 : m$ and θ . Then, by direct calculations, we have

$$\nabla^2 \mathcal{L}(\theta) = A + \Pi \text{diag}(\nabla^2 f_1, \nabla^2 f_2, \dots, \nabla^2 f_m) \Pi^T = \Pi \text{diag}(\Pi_1 A \Pi_1^T + \nabla^2 f_1, \dots, \Pi_m A \Pi_m^T + \nabla^2 f_m) \Pi.$$

That is, under the above conditions, Equation (34) provides a general example of a non-quadratic loss satisfying $\delta = \Pi_i \nabla^2 \mathcal{L}(\theta) \Pi_j^T = 0$ for all $i \neq j$.

In addition, the small cross-spectrum is pertinent in the case of local convergence. Specifically, we express $\nabla^2 \mathcal{L}(\theta) = \nabla^2 \mathcal{L}(\theta^*) + (\nabla^2 \mathcal{L}(\theta) - \nabla^2 \mathcal{L}(\theta^*))$ and take Π to be the eigenvectors of $\nabla^2 \mathcal{L}(\theta^*)$, then the cross-spectrum is given by $\|\Pi_i (\nabla^2 \mathcal{L}(\theta) - \nabla^2 \mathcal{L}(\theta^*)) \Pi_j^T\|$, which can be sufficiently small if θ is very close to θ^* , the global minimizer of the loss $\mathcal{L}(\theta)$.

4. Conclusion

This paper shows that multiscale data leads to empirical loss functions whose gradients and Hessians inherit the multiscale properties. Utilizing these properties, the introduced explicit MrGD scheme converges with a near-optimal rate for convex problems. The theories developed in this work partially explain the so-called learning rate warm-up strategy employed in neural network training.

Acknowledgements

Liu and Tsai are partially supported by National Science Foundation Grant DMS-2110895. Tsai is also supported partially by Army Research Office Grant W911NF2320240. He is supported by the KAUST Baseline Research Fund.

References

- Ansuini, A., Laio, A., Macke, J. H., and Zoccolan, D. Intrinsic dimension of data representations in deep neural networks. *Advances in Neural Information Processing Systems*, 32, 2019.
- Belkin, M. and Niyogi, P. Laplacian eigenmaps for dimensionality reduction and data representation. *Neural computation*, 15(6):1373–1396, 2003.
- Brahma, P. P., Wu, D., and She, Y. Why deep learning works: A manifold disentanglement perspective. *IEEE transactions on neural networks and learning systems*, 27(10):1997–2008, 2015.
- Brand, M. Charting a manifold. *Advances in neural information processing systems*, 15, 2002.
- Brown, B. C., Caterini, A. L., Ross, B. L., Cresswell, J. C., and Loaiza-Ganem, G. Verifying the union of manifolds hypothesis for image data. In *The Eleventh International Conference on Learning Representations*, 2022.
- Carlsson, G. Topology and data. *Bulletin of the American Mathematical Society*, 46(2):255–308, 2009.
- Chen, M., Jiang, H., Liao, W., and Zhao, T. Efficient approximation of deep relu networks for functions on low dimensional manifolds. *Advances in neural information processing systems*, 32, 2019.
- Cloninger, A. and Klock, T. A deep network construction that adapts to intrinsic dimensionality beyond the domain. *Neural Networks*, 141:404–419, 2021.
- Das Gupta, S., Van Parys, B. P., and Ryu, E. K. Branch-and-bound performance estimation programming: a unified methodology for constructing optimal optimization methods. *Mathematical Programming*, pp. 1–73, 2023.
- Donoho, D. L. and Grimes, C. Hessian eigenmaps: Locally linear embedding techniques for high-dimensional data. *Proceedings of the National Academy of Sciences*, 100(10):5591–5596, 2003.
- Du, S. S., Zhai, X., Póczos, B., and Singh, A. Gradient descent provably optimizes over-parameterized neural networks. *arXiv preprint arXiv:1810.02054*, 2018.

- Engquist, B. and Tsai, Y.-H. Heterogeneous multiscale methods for stiff ordinary differential equations. *Mathematics of computation*, 74(252):1707–1742, 2005.
- Fefferman, C., Mitter, S., and Narayanan, H. Testing the manifold hypothesis. *Journal of the American Mathematical Society*, 29(4):983–1049, 2016.
- Glorot, X. and Bengio, Y. Understanding the difficulty of training deep feedforward neural networks. In *Proceedings of the thirteenth international conference on artificial intelligence and statistics*, pp. 249–256. JMLR Workshop and Conference Proceedings, 2010.
- Grimmer, B. Provably faster gradient descent via long steps. *arXiv preprint arXiv:2307.06324*, 2023.
- Hackbusch, W. *Multi-grid methods and applications*, volume 4. Springer Science & Business Media, 2013.
- He, H., Huang, G., and Yuan, Y. Asymmetric valleys: Beyond sharp and flat local minima. *Advances in neural information processing systems*, 32, 2019.
- He, J., Tsai, R., and Ward, R. Side effects of learning from low-dimensional data embedded in a euclidean space. *Research in the Mathematical Sciences*, 10(1):13, 2023.
- He, K., Zhang, X., Ren, S., and Sun, J. Delving deep into rectifiers: Surpassing human-level performance on imagenet classification. In *Proceedings of the IEEE international conference on computer vision*, pp. 1026–1034, 2015.
- Hestenes, M. R., Stiefel, E., et al. Methods of conjugate gradients for solving linear systems. *Journal of research of the National Bureau of Standards*, 49(6):409–436, 1952.
- Hotelling, H. Analysis of a complex of statistical variables into principal components. *Journal of educational psychology*, 24(6):417, 1933.
- Jacot, A., Gabriel, F., and Hongler, C. Neural tangent kernel: Convergence and generalization in neural networks. *Advances in neural information processing systems*, 31, 2018.
- Kong, L. and Tao, M. Stochasticity of deterministic gradient descent: Large learning rate for multiscale objective function. *Advances in Neural Information Processing Systems*, 33:2625–2638, 2020.
- Krizhevsky, A., Hinton, G., et al. Learning multiple layers of features from tiny images. 2009.
- Lee, Y.-J., Wu, J., Xu, J., and Zikatanov, L. Robust subspace correction methods for nearly singular systems. *Mathematical Models and Methods in Applied Sciences*, 17(11):1937–1963, 2007.
- Li, X., Lu, F., Tao, M., and Ye, F. X.-F. Nysalt: Nyström-type inference-based schemes adaptive to large time-stepping. *Journal of Computational Physics*, 477:111952, 2023.
- Liu, L., Jiang, H., He, P., Chen, W., Liu, X., Gao, J., and Han, J. On the variance of the adaptive learning rate and beyond. In *International Conference on Learning Representations*, 2020.
- Liu, L., He, J., and Tsai, R. Linear regression on manifold structured data: the impact of extrinsic geometry on solutions. *arXiv preprint arXiv:2307.02478*, 2023.
- Loshchilov, I. and Hutter, F. Sgdr: Stochastic gradient descent with warm restarts. In *International Conference on Learning Representations*, 2017.
- Ma, C., Kunin, D., Wu, L., and Ying, L. Beyond the quadratic approximation: the multiscale structure of neural network loss landscapes. *arXiv preprint arXiv:2204.11326*, 2022.
- Manteuffel, T. A. The tchebychev iteration for nonsymmetric linear systems. *Numerische Mathematik*, 28:307–327, 1977.
- Medina, F. P., Ness, L., Weber, M., and Djima, K. Y. Heuristic framework for multiscale testing of the multi-manifold hypothesis. *Research in Data Science*, pp. 47–80, 2019.
- Mei, S., Bai, Y., and Montanari, A. The landscape of empirical risk for nonconvex losses. *The Annals of Statistics*, 46(6A): 2747–2774, 2018.

- Narayanan, H. and Mitter, S. Sample complexity of testing the manifold hypothesis. *Advances in neural information processing systems*, 23, 2010.
- Nesterov, Y. A method for unconstrained convex minimization problem with the rate of convergence $o(1/k^2)$. In *Dokl. Akad. Nauk. SSSR*, volume 269, pp. 543, 1983.
- Niyogi, P., Smale, S., and Weinberger, S. Finding the homology of submanifolds with high confidence from random samples. *Discrete & Computational Geometry*, 39:419–441, 2008.
- Oymak, S. Provable super-convergence with a large cyclical learning rate. *IEEE Signal Processing Letters*, 28:1645–1649, 2021.
- Pearson, K. Liii. on lines and planes of closest fit to systems of points in space. *The London, Edinburgh, and Dublin philosophical magazine and journal of science*, 2(11):559–572, 1901.
- Peyré, G. Manifold models for signals and images. *Computer vision and image understanding*, 113(2):249–260, 2009.
- Polyak, B. T. Some methods of speeding up the convergence of iteration methods. *Ussr computational mathematics and mathematical physics*, 4(5):1–17, 1964.
- Pope, P., Zhu, C., Abdelkader, A., Goldblum, M., and Goldstein, T. The intrinsic dimension of images and its impact on learning. *arXiv preprint arXiv:2104.08894*, 2021.
- Robbins, H. and Monro, S. A stochastic approximation method. *The annals of mathematical statistics*, pp. 400–407, 1951.
- Roweis, S. T. and Saul, L. K. Nonlinear dimensionality reduction by locally linear embedding. *science*, 290(5500):2323–2326, 2000.
- Saul, L. K. and Roweis, S. T. Think globally, fit locally: unsupervised learning of low dimensional manifolds. *Journal of machine learning research*, 4(Jun):119–155, 2003.
- Schölkopf, B., Smola, A., and Müller, K.-R. Nonlinear component analysis as a kernel eigenvalue problem. *Neural computation*, 10(5):1299–1319, 1998.
- Schonsheck, S. C., Mahan, S., Klock, T., Cloninger, A., and Lai, R. Semi-supervised manifold learning with complexity decoupled chart autoencoders. *arXiv preprint arXiv:2208.10570*, 2022.
- Smith, L. N. and Topin, N. Super-convergence: Very fast training of neural networks using large learning rates. In *Artificial intelligence and machine learning for multi-domain operations applications*, volume 11006, pp. 369–386. SPIE, 2019.
- Tao, M., Owhadi, H., and Marsden, J. E. Nonintrusive and structure preserving multiscale integration of stiff odes, sdes, and hamiltonian systems with hidden slow dynamics via flow averaging. *Multiscale Modeling & Simulation*, 8(4):1269–1324, 2010.
- Tenenbaum, J. B., Silva, V. d., and Langford, J. C. A global geometric framework for nonlinear dimensionality reduction. *science*, 290(5500):2319–2323, 2000.
- Tiwari, S. and Konidaris, G. Effects of data geometry in early deep learning. *Advances in Neural Information Processing Systems*, 35:30099–30113, 2022.
- Wang, X. and Yuan, Y.-x. On the convergence of stochastic gradient descent with bandwidth-based step size. *Journal of Machine Learning Research*, 24(48):1–49, 2023.
- Wang, Y., Chen, M., Zhao, T., and Tao, M. Large learning rate tames homogeneity: Convergence and balancing effect. In *International Conference on Learning Representations*, 2022.
- Weinberger, K. Q. and Saul, L. K. Unsupervised learning of image manifolds by semidefinite programming. *International journal of computer vision*, 70:77–90, 2006.
- Wu, L., Ma, C., et al. How sgd selects the global minima in over-parameterized learning: A dynamical stability perspective. *Advances in Neural Information Processing Systems*, 31, 2018.

- Xu, J. Iterative methods by space decomposition and subspace correction. *SIAM review*, 34(4):581–613, 1992.
- Xu, J. and Zikatanov, L. Algebraic multigrid methods. *Acta Numerica*, 26:591–721, 2017.
- You, K., Long, M., Wang, J., and Jordan, M. I. How does learning rate decay help modern neural networks? *arXiv preprint arXiv:1908.01878*, 2019.

A. Notations for the proofs

Here we list out some notations we used for the proofs in the appendices.

Notation A.1. Let z be a function of (\mathbf{x}, g) or a random variable in \mathbb{R}^m or $\mathbb{R}^{m \times n}$ over some probability space and let z_i denote a sample realization of z . We denote the empirical average on the whole dataset

$$\langle z \rangle_N := \frac{1}{N} \sum_{i=1}^N z((\mathbf{x}_i, g)),$$

the average on the mini-batch $\mathcal{B} \subset \mathcal{D}$

$$\langle z \rangle_{\mathcal{B}} := \frac{1}{|\mathcal{B}|} \sum_{(\mathbf{x}, g) \in \mathcal{B}} z((\mathbf{x}, g)),$$

and the mean

$$\langle z \rangle := \lim_{N \rightarrow \infty} \langle z \rangle_N = \mathbb{E}[z].$$

Notation A.2. Here, we introduce some commonly used products for tensors to simplify our notation. For simplicity, we only introduce these products under special cases, which will appear in the following sections. For any r -th order tensor $A \in \mathbb{R}^{n_1 \times n_2 \times \dots \times n_r}$, let us use

$$[A]_{i_1, i_2, \dots, i_r}, \quad i_1 = 1 : n_1, i_2 = 1 : n_2, \dots, i_r = 1 : n_r \quad (35)$$

to define elements in A with index (i_1, i_2, \dots, i_r) for $i_1 = 1 : n_1, i_2 = 1 : n_2, \dots, i_r = 1 : n_r$.

Tensor contraction: Let $A \in \mathbb{R}^{n_1 \times n_2 \times n_r \times k}$ and $B \in \mathbb{R}^{k \times m_1 \times m_2 \times m_s}$, we denote the tensor contraction $A \cdot B \in \mathbb{R}^{n_1 \times \dots \times n_r \times m_1 \times \dots \times m_s}$ as

$$[A \cdot B]_{i_1, \dots, i_r, j_1, \dots, j_s} = \sum_{t=1}^k [A]_{i_1, \dots, i_r, t} [B]_{t, j_1, \dots, j_s} \quad (36)$$

which then becomes a 2nd order tensor.

Tenor production: Let $A \in \mathbb{R}^{n \times m}$ and $b \in \mathbb{R}^k$, we denote the tensor production $A \otimes b \in \mathbb{R}^{n \times m \times k}$ as

$$[A \otimes b]_{i, j, k} = [A]_{i, j} [b]_k, \quad i = 1 : n, j = 1 : m, k = 1 : k, \quad (37)$$

which then becomes a 3rd order tensor.

Hadamard product: Let $a, b \in \mathbb{R}^k$, we denote the Hadamard product $a \odot b \in \mathbb{R}^k$ as

$$[a \odot b]_s = [a]_s [b]_s, \quad s = 1 : k, \quad (38)$$

which is still a 1st order tensor.

Notation A.3. Here we denote some norms for vector and matrix spaces. For vectors, we denote the ℓ^p norm of vector $a \in \mathbb{R}^d$ as

$$\|a\|_p := \left(\sum_{i=1}^d |a_i|^p \right)^{\frac{1}{p}} \quad (39)$$

for all $1 \leq p \leq \infty$. In particular, we have

$$\|a\|_{\infty} := \max_i \{|a_i|\}. \quad (40)$$

For simplicity, we define $\|a\| := \|a\|_2$ for vectors.

For matrix, we introduce only the ℓ^2 norm for any $A \in \mathbb{R}^{n \times m}$ as

$$\|A\| = \sup_{b \in \mathbb{R}^m, \|b\| \leq 1} \frac{\|Ab\|}{\|b\|}. \quad (41)$$

Lemma A.1. For any $a \in \mathbb{R}^d$, we have

$$\|a\|_{\infty} \leq \|a\| \leq \|a\|_1 \leq n \|a\|_{\infty}. \quad (42)$$

Remark A.2. For any $a \in \mathbb{R}^{1 \times d}$, which can be understood as either a matrix or a vector, the ℓ^2 matrix norm is consistent with the ℓ^2 vector norm. By abuse of notation, we will always use $\|\cdot\|$ for ℓ^2 norm for both vectors and matrices.

B. Multiscale structure of gradient flow in DNNs

In this section, we showcase that there exists the same structure in the gradient flow of DNNs compared to linear and logistic regressions when data have the same multiscale structure. For simplicity, let us first prove the result for data with two scales. Then, we generalize our results to multiscale data by induction.

B.1. Two-scale structure of gradient flow in DNNs

For data with two scales, we assume the data points concentrate around a low-dimensional subspace with a small variance in the orthogonal complement. More specifically,

$$\mathbf{x}_i = \begin{pmatrix} x_i^0 \\ \varepsilon x_i^1 \end{pmatrix} \in \mathbb{R}^{d_0+d_1}, \quad (43)$$

where $x_i^0 \sim \mathcal{U}_x \in \mathbb{R}^{d_0}$, $x_i^1 \sim \mathcal{U}([-1, 1]^{d_1}) \in \mathbb{R}^{d_1}$, and $0 \leq \varepsilon \ll 1$. Following the notation above, we have

$$\mathbf{x}^0 = \begin{pmatrix} x^0 \\ 0 \end{pmatrix}, \quad \mathbf{x}^1 = \begin{pmatrix} x^0 \\ \varepsilon x^1 \end{pmatrix} = \mathbf{x}. \quad (44)$$

In the rest of this subsection, we prove the two-scale structure of the gradient flow for DNNs. First, have

$$\frac{\partial \mathcal{L}}{\partial W^\ell} = \left\langle (f(\mathbf{x}; \theta) - g) \frac{\partial f}{\partial f^\ell} \cdot \frac{\partial f^\ell}{\partial W^\ell} \right\rangle_N, \quad (45)$$

where $\frac{\partial f}{\partial f^\ell} \cdot \frac{\partial f^\ell}{\partial W^\ell} \in \mathbb{R}^{n_\ell \times n_{\ell-1}}$ denotes the tensor contraction between the 1st order tensor $\frac{\partial f}{\partial f^\ell} \in \mathbb{R}^{n_\ell}$ and the 3rd order tensor $\frac{\partial f^\ell}{\partial W^\ell} \in \mathbb{R}^{n_\ell \times n_\ell \times n_{\ell-1}}$ as in Equation (36).

For $\frac{\partial f^\ell}{\partial W^\ell}$, we have

$$\frac{\partial f^\ell(\mathbf{x})}{\partial W^\ell} = \text{diag}(D^\ell(\mathbf{x})) \otimes f^{\ell-1}(\mathbf{x}), \quad (46)$$

where

$$D^\ell(\mathbf{x}) = \sigma'(W^\ell f^{\ell-1}(\mathbf{x}) + b^\ell) \in \mathbb{R}^{n_\ell} \quad (47)$$

and \otimes denotes the tensor product as in Equation (37). Furthermore, let us denote

$$\lambda^\ell(\mathbf{x}) = \frac{\partial f}{\partial f^\ell} \Big|_{\mathbf{x}}. \quad (48)$$

Given the properties of the tensor product and standard matrix/vector product, we have

$$\frac{\partial f}{\partial f^\ell} \cdot \frac{\partial f^\ell}{\partial W^\ell} = \lambda^\ell(\mathbf{x}) \cdot \text{diag}(D^\ell(\mathbf{x})) \otimes f^{\ell-1}(\mathbf{x}) = (\lambda^\ell(\mathbf{x}) \odot D^\ell(\mathbf{x})) (f^{\ell-1}(\mathbf{x}))^T, \quad (49)$$

where \odot denotes the Hadamard product as in Equation (38). Here, $\lambda^\ell(\mathbf{x}) \odot D^\ell(\mathbf{x})$ will be the element-wise product with two vectors in \mathbb{R}^{n_ℓ} . We further denote

$$\tilde{\lambda}^\ell(\mathbf{x}) = \lambda^\ell(\mathbf{x}) \odot D^\ell(\mathbf{x}) \in \mathbb{R}^{n_\ell}. \quad (50)$$

Consequently, we can rewrite $\frac{\partial \mathcal{L}}{\partial W^\ell}$ as

$$\frac{\partial \mathcal{L}}{\partial W^\ell} = \left\langle (f(\mathbf{x}; \theta) - g) \tilde{\lambda}^\ell(\mathbf{x}) (f^{\ell-1}(\mathbf{x}))^T \right\rangle_N \quad (51)$$

B.1.1. TWO-SCALE DECOMPOSITION OF f^ℓ

We first show the two-scale structures in the forward propagation process in DNNs with general activation functions.

Lemma B.1. For any DNN defined in Equation (6) and dataset with two scales as in Equation (43) under Assumption 2.1, we have

$$f^\ell(\mathbf{x}) = f_0^\ell(\mathbf{x}^0) + \varepsilon f_1^\ell(\mathbf{x}^1), \quad \ell = 1 : L \quad (52)$$

where

$$f_0^\ell(\mathbf{x}^0) = f^\ell(\mathbf{x}^0) = f^\ell \left(\begin{pmatrix} x \\ 0 \end{pmatrix} \right) \quad (53)$$

and

$$\|f_1^\ell(\mathbf{x}^1)\| \leq (\text{Lip}(\sigma))^\ell \|W_1^1 x^1\| \prod_{k=2}^{\ell} \|W^k\|, \quad (54)$$

where $\text{Lip}(\sigma)$ denotes the Lipschitz constant of activation function σ .

Proof. We use proof by induction. For $\ell = 1$, we have

$$f^1(\mathbf{x}) = \sigma(W_0^1 x^0 + b^1 + \varepsilon W_1^1 x^1), \quad (55)$$

where $W^1 = \begin{pmatrix} W_0^1 \\ W_1^1 \end{pmatrix}$ and W_0^1, W_1^1 correspond to the x^0, x^1 components of \mathbf{x} respectively. We first define

$$f_0^1(\mathbf{x}^0) = \sigma(W_0^1 x^0 + b^1) = f^1(\mathbf{x}^0) = f^1 \left(\begin{pmatrix} x \\ 0 \end{pmatrix} \right). \quad (56)$$

Then, we have

$$\begin{aligned} [f^1(\mathbf{x}) - f_0^1(\mathbf{x}^0)]_i &= [\sigma(W_0^1 x^0 + b^1 + \varepsilon W_1^1 x^1) - \sigma(W_0^1 x^0 + b^1)]_i \\ &= \varepsilon \sigma'(\xi_{[W^1 \mathbf{x} + b^1]_i, [W_1^1 \varepsilon x^1]_i}) [W_1^1 x^1]_i, \end{aligned} \quad (57)$$

where $\xi_{[W^1 \mathbf{x} + b^1]_i, [W_1^1 \varepsilon x^1]_i}$ depends on $[W^1 \mathbf{x} + b^1]_i$, and $[W_1^1 \varepsilon x^1]_i$. Since εx^1 is a part of $\mathbf{x}^1 = \begin{pmatrix} x^0 \\ \varepsilon x^1 \end{pmatrix} = \mathbf{x}$, it means that $\xi_{[W^1 \mathbf{x} + b^1]_i, [W_1^1 \varepsilon x^1]_i}$ depends on \mathbf{x}^1 with parameters W^1 and b^1 which are parts of θ . Thus, we can write

$$f^1(\mathbf{x}) - f_0^1(\mathbf{x}^0) = \varepsilon f_1^1(\mathbf{x}^1; \theta) = \varepsilon f_1^1(\mathbf{x}^1). \quad (58)$$

Moreover, we have

$$\|\varepsilon f_1^1(\mathbf{x}^1)\| = \|\sigma(W_0^1 x^0 + b^1 + \varepsilon W_1^1 x^1) - \sigma(W_0^1 x^0 + b^1)\| \leq \varepsilon \text{Lip}(\sigma) \|W_1^1 x^1\|. \quad (59)$$

This finishes the proof for $\ell = 1$. Note that $f_1^1(\mathbf{x}^1)$ depends also on the previous scale such that $f_1^1(\mathbf{x}^1) = f_1^1(\mathbf{x}_0, \mathbf{x}_1)$, but for brevity we only include the component corresponding to the smallest scale. The same convention will be adopted throughout the rest of the proof.

We prove them by induction for $\ell > 1$. Now, we assume that results hold for $1, 2, \dots, \ell - 1$, let us prove it for ℓ . According to the definition and assumption for $\ell - 1$, we have

$$f^\ell(\mathbf{x}) = \sigma(W^\ell f^{\ell-1}(\mathbf{x}) + b^\ell) = \sigma(W^\ell (f_0^{\ell-1}(\mathbf{x}^0) + \varepsilon f_1^{\ell-1}(\mathbf{x}^1)) + b^\ell). \quad (60)$$

Similarly, we have

$$f_0^\ell(\mathbf{x}^0) := \sigma(W^\ell f_0^{\ell-1}(\mathbf{x}^0) + b^\ell) = \sigma(W^\ell f^{\ell-1}(\mathbf{x}^0) + b^\ell) = f^\ell(\mathbf{x}^0). \quad (61)$$

Again,

$$\begin{aligned} [f^\ell(\mathbf{x}) - f_0^\ell(\mathbf{x}^0)]_i &= [\sigma(W^\ell f_0^{\ell-1}(\mathbf{x}^0) + b^1 + \varepsilon f_1^{\ell-1}(\mathbf{x}^1)) - \sigma(W^\ell f_0^{\ell-1}(\mathbf{x}^0) + b^1)]_i \\ &= \varepsilon \sigma'(\xi_{[W^\ell f_0^{\ell-1}(\mathbf{x}^0) + b^\ell]_i, [\varepsilon f_1^{\ell-1}(\mathbf{x}^1)]_i}) [W_1^1 x^1]_i \\ &= \varepsilon f_1^\ell(\mathbf{x}^1; \theta) = \varepsilon f_1^\ell(\mathbf{x}^1). \end{aligned} \quad (62)$$

Furthermore, we have

$$\begin{aligned} \|\varepsilon f_1^\ell\| &= \|\sigma(W^\ell (f_0^{\ell-1}(\mathbf{x}^0) + \varepsilon f_1^{\ell-1}(\mathbf{x}^1)) + b^\ell) - \sigma(W^\ell f_0^{\ell-1}(\mathbf{x}^0) + b^\ell)\| \\ &\leq \varepsilon \text{Lip}(\sigma) \|W^\ell f_1^{\ell-1}(\mathbf{x}^1)\| \\ &\leq \varepsilon \text{Lip}(\sigma) \|W^\ell\| \|f_1^{\ell-1}(\mathbf{x}^1)\|. \end{aligned} \quad (63)$$

Finally, we have the bound for $\|f_1^\ell(\mathbf{x}^1)\|$ by induction. \square

B.1.2. TWO-SCALE STRUCTURE IN $\tilde{\lambda}^\ell$.

Recall that $\frac{\partial \mathcal{L}}{\partial W^\ell} = \left\langle (f(\mathbf{x}; \theta) - g) \tilde{\lambda}^\ell(\mathbf{x}) (f^{\ell-1}(\mathbf{x}))^T \right\rangle_N$, we will study the two-scale structure in $\lambda^\ell(\mathbf{x})$ and $\tilde{\lambda}^\ell$ in this subsection. Before that, we first have the following two-scale structure in $D^\ell(\mathbf{x}) := \sigma'(W^\ell f^{\ell-1}(\mathbf{x}) + b^\ell) \in \mathbb{R}^{n_\ell}$.

Lemma B.2. *For any DNN defined in Equation (6) and dataset with two scales as in Equation (43) under Assumption 2.1, we have*

$$D^\ell(\mathbf{x}) = D_0^\ell(\mathbf{x}^0) + \varepsilon D_1^\ell(\mathbf{x}^1), \quad \ell = 1 : L. \quad (64)$$

In particular, we have

$$D_0^\ell(\mathbf{x}^0) = \sigma'(W^\ell f_0^{\ell-1}(\mathbf{x}^0) + b^\ell) = \sigma'(W^\ell f^{\ell-1}(\mathbf{x}^0) + b^\ell) = D^\ell(\mathbf{x}^0), \quad (65)$$

and

$$\|D_1^\ell(\mathbf{x}^1)\| \leq \text{Lip}(\sigma') (\text{Lip}(\sigma))^{\ell-1} \|W_1^1 x^1\| \prod_{k=2}^{\ell} \|W^k\|. \quad (66)$$

Proof. Given $\sigma \in C^2$ and the decomposition of $f^\ell(\mathbf{x})$ in Lemma B.1, we have

$$\begin{aligned} D^\ell(\mathbf{x}) &= \sigma'(W^\ell f^{\ell-1}(\mathbf{x}) + b^\ell) \\ &= \sigma'(W^\ell f_0^{\ell-1}(\mathbf{x}^0) + b^\ell + \varepsilon W^\ell f_1^{\ell-1}(\mathbf{x}^1)) \\ &= \sigma'(W^\ell f^{\ell-1}(\mathbf{x}^0) + b^\ell) + \varepsilon \text{diag}(\sigma''(\xi)) W^\ell f_1^{\ell-1}(\mathbf{x}^1) \\ &= D_0^\ell(\mathbf{x}^0) + \varepsilon D_1^\ell(\mathbf{x}^1; \theta) \\ &= D^\ell(\mathbf{x}^0) + \varepsilon D_1^\ell(\mathbf{x}^1), \end{aligned} \quad (67)$$

where $\xi \in \mathbb{R}^{n_\ell}$ and each $[\xi]_i$ is determined by $[W^\ell f_0^{\ell-1}(\mathbf{x}^0) + b^\ell]_i$, and $\varepsilon [W^\ell f_1^{\ell-1}(\mathbf{x}^1)]_i$ via the intermediate value theorem. In addition, we have the following bound

$$\begin{aligned} \|\varepsilon D_1^\ell\| &= \|\sigma'(W^\ell f_0^{\ell-1}(\mathbf{x}^0) + b^\ell + \varepsilon W^\ell f_1^{\ell-1}(\mathbf{x}^1)) - \sigma'(W^\ell f_0^{\ell-1}(\mathbf{x}^0) + b^\ell)\| \\ &\leq \varepsilon \text{Lip}(\sigma') \|W^\ell f_1^{\ell-1}(\mathbf{x}^1)\| \\ &\leq \varepsilon \text{Lip}(\sigma') (\text{Lip}(\sigma))^{\ell-1} \|W_1^1 x^1\| \prod_{k=2}^{\ell} \|W^k\|. \end{aligned} \quad (68)$$

□

Corollary B.3. *We have*

$$\|\text{diag}(D_1^\ell)\| \leq \|D_1^\ell\|. \quad (69)$$

Proof. Given the properties of matrix norm and vector norm, we have

$$\|\text{diag}(D_1^\ell)\| = \|D_1^\ell\|_\infty \leq \|D_1^\ell\|. \quad (70)$$

□

Based on the two-scale structure in $D^\ell(\mathbf{x})$, we have the following two-scale structure for $\lambda^\ell(\mathbf{x})$.

Lemma B.4. *For any DNN defined in Equation (6) and dataset with two scales as in Equation (43) under Assumption 2.1, we have*

$$\lambda^\ell(\mathbf{x}) = \lambda_0^\ell(\mathbf{x}^0) + \varepsilon \lambda_1^\ell(\mathbf{x}^1), \quad \ell = 1 : L \quad (71)$$

where

$$(\lambda_0^\ell(\mathbf{x}^0))^T = \frac{\partial f}{\partial f^\ell} \Big|_{\mathbf{x}^0} = (\lambda^\ell(\mathbf{x}^0))^T = W^{L+1} \prod_{k=\ell+1}^L (\text{diag}(D_0^k(\mathbf{x}^0)) W^k). \quad (72)$$

In particular, we have the following recursive definitions of $\lambda_0^\ell(\mathbf{x}^0)$ and $\lambda_1^\ell(\mathbf{x}^1)$:

$$(\lambda_0^\ell(\mathbf{x}^0))^T = (\lambda_0^{\ell+1}(\mathbf{x}^0))^T \text{diag}(D_0^{\ell+1}(\mathbf{x}^0)) W^{\ell+1} \quad (73)$$

and

$$\begin{aligned} (\lambda_1^\ell(\mathbf{x}^1))^T &= (\lambda_1^\ell(\mathbf{x}^1; \theta, \varepsilon))^T \\ &= (\lambda_1^{\ell+1}(\mathbf{x}^1))^T \text{diag}(D_0^{\ell+1}(\mathbf{x}^0)) W^{\ell+1} \\ &\quad + (\lambda_0^{\ell+1}(\mathbf{x}^0))^T (\text{diag}(D_1^{\ell+1}(\mathbf{x}^1)) W^{\ell+1}) \\ &\quad + \varepsilon (\lambda_1^{\ell+1}(\mathbf{x}^1))^T \text{diag}(D_1^{\ell+1}(\mathbf{x}^1)) W^{\ell+1}, \end{aligned} \quad (74)$$

with

$$(\lambda_0^L(\mathbf{x}^0))^T = W^{L+1} \quad \text{and} \quad \lambda_1^L(\mathbf{x}^1) = 0. \quad (75)$$

Furthermore, we have the explicit upper bound for $\|\lambda_1^\ell\|$ as

$$\|\lambda_1^\ell\| \leq \|W^{L+1}\| \prod_{k=\ell+1}^L \|W^k\| \left(\sum_{\ell+1 \leq i \leq L} \|D_1^i\| \prod_{\ell+1 \leq k \neq i \leq L} \|D_0^k\| \right) + \mathcal{O}(\varepsilon). \quad (76)$$

Proof. We prove it by induction. For λ^L , by definition, we have

$$(\lambda^L(\mathbf{x}))^T = \left(\frac{\partial f}{\partial f^L} \right)^T = W^{L+1}. \quad (77)$$

To make Equation (71) holds for $\ell = L$, we define $(\lambda_0^L(\mathbf{x}^0))^T = W^{L+1}$ and $\lambda_1^L(\mathbf{x}^1) = 0$. Thus, for any $1 \leq \ell < L$,

$$(\lambda^\ell(\mathbf{x}))^T = \left(\frac{\partial f}{\partial f^{\ell+1}} \cdot \frac{\partial f^{\ell+1}}{\partial f^\ell} \right)^T = (\lambda^{\ell+1}(\mathbf{x}))^T \text{diag}(D^{\ell+1}(\mathbf{x})) W^{\ell+1}. \quad (78)$$

Given the decomposition of $D^{\ell+1}(\mathbf{x})$ in Lemma B.2 and $\lambda^{\ell+1}(\mathbf{x})$ in Equation (71), we have

$$\begin{aligned} &(\lambda^\ell(\mathbf{x}))^T \\ &= (\lambda_0^{\ell+1}(\mathbf{x}^0) + \varepsilon \lambda_1^{\ell+1}(\mathbf{x}^1))^T \text{diag}(D_0^{\ell+1}(\mathbf{x}^0) + \varepsilon D_1^{\ell+1}(\mathbf{x}^1)) W^{\ell+1} \\ &= (\lambda_0^{\ell+1}(\mathbf{x}^0))^T \text{diag}(D_0^{\ell+1}(\mathbf{x}^0)) W^{\ell+1} \\ &\quad + \varepsilon \left((\lambda_1^{\ell+1}(\mathbf{x}^1))^T \text{diag}(D_0^{\ell+1}(\mathbf{x}^0)) \right. \\ &\quad \left. + (\lambda_0^{\ell+1}(\mathbf{x}^0))^T (\text{diag} D_1^{\ell+1}(\mathbf{x}^1)) \right. \\ &\quad \left. + \varepsilon (\lambda_1^{\ell+1}(\mathbf{x}^1))^T \text{diag}(D_1^{\ell+1}(\mathbf{x}^1)) \right) W^{\ell+1} \\ &= \lambda_0^\ell(\mathbf{x}^0) + \varepsilon \lambda_1^\ell(\mathbf{x}^1; \theta, \varepsilon). \end{aligned} \quad (79)$$

Thus, we obtain the recursive formula for $\lambda_0^\ell(\mathbf{x}^0)$ and $\lambda_1^\ell(\mathbf{x}^1)$. To explicitly bound $\lambda_1^\ell(\mathbf{x}^1)$, we apply the recursion repeatedly and have

$$(\lambda_1^\ell)^T = W^{L+1} \sum_{\ell+1 \leq i \leq L} \widetilde{\prod}_{\ell+1 \leq k \neq i \leq L} (\text{diag}(D_1^i) W^i (\text{diag}(D_0^k) W^k)) + \mathcal{O}(\varepsilon). \quad (80)$$

Noticing the non-commutativity of the multiplication of matrices, we denote

$$\begin{aligned} &\widetilde{\prod}_{\ell+1 \leq k \neq i \leq L} (\text{diag}(D_1^i) W^i (\text{diag}(D_0^k) W^k)) \\ &= \text{diag}(D_0^L) W^L \dots \\ &\quad \text{diag}(D_0^{i+1}) W^{i+1} \text{diag}(D_1^i) W^i \text{diag}(D_0^{i-1}) W^{i-1} \\ &\quad \dots \text{diag}(D_0^{\ell+1}) W^{\ell+1}. \end{aligned} \quad (81)$$

Thus, we can bound $\|\lambda_1^\ell\|$ by

$$\|\lambda_1^\ell\| \leq \|W^{L+1}\| \prod_{k=\ell+1}^L \|W^k\| \left(\sum_{\ell+1 \leq i \leq L} \|D_1^i\| \prod_{\ell+1 \leq k \neq i \leq L} \|D_0^k\| \right) + \mathcal{O}(\varepsilon). \quad (82)$$

□

Corollary B.5. For $\tilde{\lambda}^\ell(\mathbf{x}) = \lambda^\ell(\mathbf{x}) \odot D^\ell(\mathbf{x}) \in \mathbb{R}^{n_\ell}$, we have

$$\tilde{\lambda}^\ell(\mathbf{x}) = \tilde{\lambda}_0^\ell(\mathbf{x}^0) + \varepsilon \tilde{\lambda}_1^\ell(\mathbf{x}^1) \quad (83)$$

where

$$\tilde{\lambda}_0^\ell(\mathbf{x}^0) = \lambda_0^\ell(\mathbf{x}^0) \odot D_0^\ell(\mathbf{x}^0) = \tilde{\lambda}^\ell(\mathbf{x}^0) \quad (84)$$

and

$$\|\tilde{\lambda}_1^\ell(\mathbf{x}^1)\| \leq \|\lambda_0^1(\mathbf{x}^0)\| \|D_1^\ell(\mathbf{x}^1)\| + \|\lambda_1^\ell(\mathbf{x}^1)\| \|D_0^\ell(\mathbf{x}^0)\| + \mathcal{O}(\varepsilon). \quad (85)$$

Proof. Given Lemma B.4 of λ^ℓ and Lemma B.2 of D^ℓ , we have

$$\begin{aligned} \tilde{\lambda}^\ell(\mathbf{x}) &= \lambda^\ell(\mathbf{x}) \odot D^\ell(\mathbf{x}) \\ &= (\lambda_0^\ell(\mathbf{x}^0) + \varepsilon \lambda_1^\ell(\mathbf{x}^1)) \odot (D_0^\ell(\mathbf{x}^0) + \varepsilon D_1^\ell(\mathbf{x}^1)) \\ &= \lambda_0^\ell(\mathbf{x}^0) \odot D_0^\ell(\mathbf{x}^0) + \varepsilon (\lambda_0^1(\mathbf{x}^0) \odot D_1^\ell(\mathbf{x}^1) + \lambda_1^\ell(\mathbf{x}^1) \odot D_0^\ell(\mathbf{x}^0) + \varepsilon \lambda_1^\ell(\mathbf{x}^1) \odot D_1^\ell(\mathbf{x}^1)) \\ &= \tilde{\lambda}_0^\ell(\mathbf{x}^0) + \varepsilon \tilde{\lambda}_1^\ell(\mathbf{x}^1; \theta, \varepsilon). \end{aligned} \quad (86)$$

Consequently, we have

$$\begin{aligned} \|\tilde{\lambda}_1^\ell(\mathbf{x}^1)\| &= \|\lambda_0^1(\mathbf{x}^0) \odot D_1^\ell(\mathbf{x}^1) + \lambda_1^\ell(\mathbf{x}^1) \odot D_0^\ell(\mathbf{x}^0) + \varepsilon \lambda_1^\ell(\mathbf{x}^1) \odot D_1^\ell(\mathbf{x}^1)\| \\ &\leq \|\lambda_0^1(\mathbf{x}^0)\| \|D_1^\ell(\mathbf{x}^1)\| + \|\lambda_1^\ell(\mathbf{x}^1)\| \|D_0^\ell(\mathbf{x}^0)\| + \mathcal{O}(\varepsilon). \end{aligned} \quad (87)$$

□

B.1.3. TWO-SCALE STRUCTURE IN DATASET \mathcal{D}

Before we study the two-scale structure of the gradient flow of DNNs on dataset \mathcal{D} , we also need to show the two-scale structure of the dataset depending on the two-scale structure of \mathbf{x} and the properties of the target $g(\mathbf{x})$.

Lemma B.6. For any $g \in C^1(\Omega)$ with $\Omega \subset \mathbb{R}^d$, and \mathbf{x} with two scales under Assumption 2.1, there exists a continuous function $g_1 : \mathbb{R}^d \mapsto \mathbb{R}$ such that

$$g(\mathbf{x}) = g_0(\mathbf{x}^0) + \varepsilon g_1(\mathbf{x}^1), \quad (88)$$

where $g_0(\mathbf{x}^0) = g(\mathbf{x}^0)$ and $\mathbf{x}^1 = \mathbf{x}$.

Proof. Use the intermediate value theorem and similar arguments shown in the proofs of Lemma B.1 and Lemma B.2. □

Given the above decomposition for the target function, we introduce the following notation

$$\begin{aligned} \left. \frac{\partial \mathcal{L}}{\partial W^\ell} \right|_{\mathcal{D}^0} &:= \frac{\partial}{\partial W^\ell} \left(\frac{1}{N} \sum_{(\mathbf{x}, g) \in \mathcal{D}^0} (f(\mathbf{x}; \theta) - g)^2 \right) \\ &= \frac{\partial}{\partial W^\ell} \left(\frac{1}{N} \sum_{i=1}^N (f(\mathbf{x}_i^0; \theta) - g(\mathbf{x}_i^0))^2 \right) \\ &= \left\langle (f(\mathbf{x}^0) - g(\mathbf{x}^0)) \tilde{\lambda}^\ell(\mathbf{x}^0) (f^{\ell-1}(\mathbf{x}^0))^T \right\rangle_{\mathcal{D}^0}. \end{aligned} \quad (89)$$

B.1.4. TWO-SCALE STRUCTURE IN $\frac{\partial \mathcal{L}}{\partial W^\ell}$.

Based on the previous decompositions and estimates, we can finally present the estimate for $\frac{\partial \mathcal{L}}{\partial W^\ell}$ as follows:

Theorem B.7. *For any DNN defined in Equation (6) and dataset \mathcal{D} with two scales as in Equation (43) under Assumption 2.1, we have*

$$\frac{\partial \mathcal{L}}{\partial W^\ell} = \langle A_0^\ell(\mathbf{x}^0) \rangle_N + \varepsilon \langle A_1^\ell(\mathbf{x}^1) \rangle_N, \quad (90)$$

where

$$\langle A_0^\ell(\mathbf{x}^0) \rangle_N = \left\langle (f(\mathbf{x}^0) - g(\mathbf{x}^0)) \tilde{\lambda}^\ell(\mathbf{x}^0) (f^{\ell-1}(\mathbf{x}^0))^T \right\rangle_{\mathcal{D}^0} = \frac{\partial \mathcal{L}}{\partial W^\ell} \Big|_{\mathcal{D}^0} \quad (91)$$

and

$$\begin{aligned} \|A_1^\ell(\mathbf{x}^1)\| &\leq |f_1(\mathbf{x}^1) - g_1(\mathbf{x}^1)| \|\tilde{\lambda}^\ell(\mathbf{x}^0)\| \|f^{\ell-1}(\mathbf{x}^0)\| \\ &\quad + |f(\mathbf{x}^0) - g(\mathbf{x}^0)| \|\tilde{\lambda}_1^\ell(\mathbf{x}^1)\| \|f^{\ell-1}(\mathbf{x}^0)\| \\ &\quad + |f(\mathbf{x}^0) - g(\mathbf{x}^0)| \|\tilde{\lambda}^\ell(\mathbf{x}^0)\| \|f_1^{\ell-1}(\mathbf{x}^1)\| + \mathcal{O}(\varepsilon). \end{aligned} \quad (92)$$

More precisely, we define

$$\begin{aligned} \langle A_1^\ell(\mathbf{x}^1) \rangle_N &:= \left\langle (f_1(\mathbf{x}^1) - g_1(\mathbf{x}^1)) \tilde{\lambda}^\ell(\mathbf{x}^0) (f^{\ell-1}(\mathbf{x}^0))^T \right\rangle_N \\ &\quad + \left\langle (f(\mathbf{x}^0) - g(\mathbf{x}^0)) \tilde{\lambda}_1^\ell(\mathbf{x}^1) (f^{\ell-1}(\mathbf{x}^0))^T \right\rangle_N \\ &\quad + \left\langle (f(\mathbf{x}^0) - g(\mathbf{x}^0)) \tilde{\lambda}^\ell(\mathbf{x}^0) (f_1^{\ell-1}(\mathbf{x}^1))^T \right\rangle_N + \langle \mathcal{O}(\varepsilon) \rangle_{\mathcal{D}^1} \end{aligned} \quad (93)$$

Proof. By definition, we have

$$\begin{aligned} \frac{\partial \mathcal{L}}{\partial W^\ell} &= \left\langle (f(\mathbf{x}) - g) \tilde{\lambda}^\ell(\mathbf{x}) (f^{\ell-1}(\mathbf{x}))^T \right\rangle_N \\ &= \left\langle (W^{L+1} f_0^L + \varepsilon W^{L+1} f_1^L - g_0 - \varepsilon g_1) (\tilde{\lambda}_0^\ell + \varepsilon \tilde{\lambda}_1^\ell) (f_0^{\ell-1} + \varepsilon f_1^{\ell-1})^T \right\rangle_N \\ &= \langle A_0^\ell(\mathbf{x}^0) \rangle_N + \varepsilon \langle A_1^\ell(\mathbf{x}^1) \rangle_N, \end{aligned} \quad (94)$$

where

$$\begin{aligned} A_0^\ell(\mathbf{x}^0) &= (W^{L+1} f_0^L - g_0) \tilde{\lambda}_0^\ell (f_0^{\ell-1})^T \\ &= (f(\mathbf{x}^0) - g(\mathbf{x}^0)) \tilde{\lambda}^\ell(\mathbf{x}^0) (f^{\ell-1}(\mathbf{x}^0))^T \end{aligned} \quad (95)$$

and

$$\begin{aligned} A_1^\ell(\mathbf{x}^1) &= (W^{L+1} f_1^L(\mathbf{x}^1) - g_1(\mathbf{x}^1)) \tilde{\lambda}_0^\ell(\mathbf{x}^0) (f_0^{\ell-1}(\mathbf{x}^0))^T \\ &\quad + (W^{L+1} f_0^L(\mathbf{x}^0) - g_0(\mathbf{x}^0)) \tilde{\lambda}_1^\ell(\mathbf{x}^1) (f_0^{\ell-1}(\mathbf{x}^0))^T \\ &\quad + (W^{L+1} f_0^L(\mathbf{x}^0) - g_0(\mathbf{x}^0)) \tilde{\lambda}_0^\ell(\mathbf{x}^0) (f_1^{\ell-1}(\mathbf{x}^1))^T + \mathcal{O}(\varepsilon) \\ &= (f_1(\mathbf{x}^1) - g_1(\mathbf{x}^1)) \tilde{\lambda}^\ell(\mathbf{x}^0) (f^{\ell-1}(\mathbf{x}^0))^T \\ &\quad + (f(\mathbf{x}^0) - g(\mathbf{x}^0)) \tilde{\lambda}_1^\ell(\mathbf{x}^1) (f^{\ell-1}(\mathbf{x}^0))^T \\ &\quad + (f(\mathbf{x}^0) - g(\mathbf{x}^0)) \tilde{\lambda}^\ell(\mathbf{x}^0) (f_1^{\ell-1}(\mathbf{x}^1))^T + \mathcal{O}(\varepsilon). \end{aligned} \quad (96)$$

As a result, we have the definition of $\langle A_1^\ell(\mathbf{x}^1) \rangle_N$ and the bound for $\|A_1^\ell(\mathbf{x}^1)\|$. □

Remark B.8. With a similar fashion, we also have the two-scale structure in $\frac{\partial \mathcal{L}}{\partial b^\ell}$ since

$$\frac{\partial \mathcal{L}}{\partial b^\ell} = \left\langle (f(\mathbf{x}; \theta) - g) \tilde{\lambda}^\ell(\mathbf{x}) \right\rangle_N. \quad (97)$$

Remark B.9. Here, we notice that \mathcal{L} can be thought as a function of ε since $\mathbf{x}_i = \begin{pmatrix} x_i^0 \\ \varepsilon x_i^1 \end{pmatrix}$. Thus, let us define

$$F^\ell(\varepsilon) = \frac{\partial \mathcal{L}(\theta; \varepsilon)}{\partial W^\ell} \in \mathbb{R}^{n_\ell \times n_{\ell-1}}. \quad (98)$$

Then, one may apply the Taylor expansion in terms of ε to $F^\ell(\varepsilon)$ and get

$$F^\ell(\varepsilon) = F^\ell(0) + \varepsilon \frac{dF^\ell(0)}{d\varepsilon} + \mathcal{O}(\varepsilon^2). \quad (99)$$

Here, we have

$$\langle A_0^\ell(x) \rangle_N = F^\ell(0), \quad \lim_{\varepsilon \rightarrow 0} \langle A_1^\ell \rangle_N = \frac{dF^\ell(0)}{d\varepsilon}. \quad (100)$$

Our previous analysis gives more precise structures and estimates for $F^\ell(0)$ and $\frac{dF^\ell(0)}{d\varepsilon}$. More important, the direct Taylor expansion for $F^\ell(\varepsilon)$ cannot be generalized to the multiscale case.

B.2. Activation functions that fit the previous analysis.

According to the previous analysis, we see that our previous analysis can be applied directly if $\text{Lip}(\sigma)$ and $\text{Lip}(\sigma')$ are uniformly bounded. For example:

Sigmoid

$$\sigma(t) = \frac{1}{1 + e^{-t}} \quad (101)$$

Tanh

$$\sigma(t) = \frac{e^t - e^{-t}}{e^t + e^{-t}} \quad (102)$$

Gaussian Error Linear Unit (GeLU)

$$\sigma(t) = t\Phi(t) = t \int_{-\infty}^t \frac{1}{\sqrt{2\pi}} e^{-\frac{s^2}{2}} ds \quad (103)$$

Softplus

$$\sigma(t) = \ln(1 + e^t) \quad (104)$$

Sigmoid linear unit (SiLU, Sigmoid shrinkage, SiL, or Swish-1)

$$\sigma(t) = \frac{t}{1 + e^{-t}} \quad (105)$$

In addition, our previous analysis can also be applied to activation functions belonging to $W_{loc}^{2,\infty}$ since we can assume $\mathbf{x} \in \Omega$, which is a bounded set and also $\|\theta\|_{\ell^2} \leq M$ in the training process.

B.3. Multiscale structure in DNNs

The key to proving the result is the extension of the multiscale decomposition for $f^\ell(\mathbf{x})$ and $D^\ell(\mathbf{x})$ (the result for $\tilde{\lambda}^\ell$ can be derived naturally based on these two results). Similar as before, we only outline the least scale components \mathbf{x}^k for clarity.

Lemma B.10. *For any DNN defined in Equation (6) and dataset under Assumption 2.1, we have*

$$f^\ell(\mathbf{x}^k) = f^\ell(\mathbf{x}^{k-1}) + \varepsilon^k f_k^\ell(\mathbf{x}^k), \quad (106)$$

and

$$D^\ell(\mathbf{x}^k) = D^\ell(\mathbf{x}^{k-1}) + \varepsilon^k D_k^\ell(\mathbf{x}^k), \quad (107)$$

for any $\ell = 1 : L$ and $k = 1 : m$. Moreover, we have

$$\|f_k^\ell(\mathbf{x}^k)\| \leq (\text{Lip}(\sigma))^\ell \|W_k^1 x^k\| \prod_{j=2}^{\ell} \|W^j\|, \quad (108)$$

and

$$\|D_k^\ell(\mathbf{x}^k)\| \leq \text{Lip}(\sigma') (\text{Lip}(\sigma))^{\ell-1} \|W_k^1 x^k\| \prod_{j=2}^{\ell} \|W^j\|. \quad (109)$$

where $\text{Lip}(\sigma)$ and $\text{Lip}(\sigma')$ denote the Lipschitz constants of activation function σ and its derivative σ' .

Proof. This is an extension of the Lemma B.1. □

Lemma B.11. For any DNN defined in Equation (6) and dataset under Assumption 2.1, we have

$$\tilde{\lambda}^\ell(\mathbf{x}^k) = \tilde{\lambda}^\ell(\mathbf{x}^{k-1}) + \varepsilon^k \tilde{\lambda}_k^\ell(\mathbf{x}^k), \quad (110)$$

where $\tilde{\lambda}_k^\ell(\mathbf{x}^k) = \tilde{\lambda}_k^\ell(\mathbf{x}^k; \theta, \varepsilon^k)$.

Similar to the two-scale decomposition of the target function in Lemma B.6, we have the following result for $g(\mathbf{x}^k)$.

Lemma B.12. For any $g \in C^1(\Omega)$ with $\Omega \subset \mathbb{R}^d$, and \mathbf{x}^m with multiscale structure under Assumption 2.1, there exists a continuous function $g_k : \mathbb{R}^d \mapsto \mathbb{R}$ such that

$$g(\mathbf{x}^k) = g(\mathbf{x}^k) + \varepsilon^k g_k(\mathbf{x}^k) \quad k = 1 : m. \quad (111)$$

Then, we define the following sets

$$\mathcal{D}^k = \{(\mathbf{x}_i^{k-1}, g(\mathbf{x}_i^{k-1}))\} \quad \text{and,} \quad k = 0 : m. \quad (112)$$

Given these new sets, we introduce the following notation

$$\begin{aligned} \left. \frac{\partial \mathcal{L}}{\partial W^\ell} \right|_{\mathcal{D}^k} &:= \frac{\partial}{\partial W^\ell} \left(\frac{1}{N} \sum_{(\mathbf{x}, g) \in \mathcal{D}^k} (f(\mathbf{x}; \theta) - g)^2 \right) \\ &= \frac{\partial}{\partial W^\ell} \left(\frac{1}{N} \sum_{i=1}^N (f(\mathbf{x}_i^k; \theta) - g(\mathbf{x}_i^k))^2 \right) \\ &= \left\langle (f(\mathbf{x}^k) - g(\mathbf{x}^k)) \tilde{\lambda}^\ell(\mathbf{x}^k) (f^{\ell-1}(\mathbf{x}^k))^T \right\rangle_N, \end{aligned} \quad (113)$$

for all $k = 0 : m$. Here, we notice that $\left. \frac{\partial \mathcal{L}}{\partial W^\ell} \right|_{\mathcal{D}^k} = \left. \frac{\partial \mathcal{L}}{\partial W^\ell} \right|_{\mathcal{D}^k} = \left. \frac{\partial \mathcal{L}}{\partial W^\ell} \right|_{\mathcal{D}^m}$.

Before the show our last theorem about the multiscale structure of the gradient flow of DNNs, we first present the following recursive decomposition for $\left. \frac{\partial \mathcal{L}(\theta)}{\partial W^\ell} \right|_{\mathcal{D}^k}$.

Lemma B.13. For any DNN defined in Equation (6) and dataset under Assumption 2.1, we have

$$\left. \frac{\partial \mathcal{L}(\theta)}{\partial W^\ell} \right|_{\mathcal{D}^k} = \left. \frac{\partial \mathcal{L}(\theta)}{\partial W^\ell} \right|_{\mathcal{D}^{k-1}} + \varepsilon^k \langle A_k^\ell(\mathbf{x}^k) \rangle_N \quad k = 1 : m, \quad (114)$$

where

$$\begin{aligned} \langle A_k^\ell(\mathbf{x}^k) \rangle_N &:= \left\langle (f_k(\mathbf{x}^k) - g_k(\mathbf{x}^k)) \tilde{\lambda}^\ell(\mathbf{x}^{k-1}) (f^{\ell-1}(\mathbf{x}^{k-1}))^T \right\rangle_N \\ &\quad + \left\langle (f(\mathbf{x}^{k-1}) - g(\mathbf{x}^{k-1})) \tilde{\lambda}_1^\ell(\mathbf{x}^k) (f^{\ell-1}(\mathbf{x}^{k-1}))^T \right\rangle_N \\ &\quad + \left\langle (f(\mathbf{x}^{k-1}) - g(\mathbf{x}^{k-1})) \tilde{\lambda}^\ell(\mathbf{x}^{k-1}) (f_k^{\ell-1}(\mathbf{x}^k))^T \right\rangle_N \\ &\quad + \langle O(\varepsilon^k) \rangle_N. \end{aligned} \quad (115)$$

More precisely, we have

$$\begin{aligned}
 \mathcal{O}(\varepsilon^k) &= \varepsilon^k \left((f(\mathbf{x}^{k-1}) - g(\mathbf{x}^{k-1})) \tilde{\lambda}_k^\ell(\mathbf{x}^k) (f_k^{\ell-1}(\mathbf{x}^k))^T \right. \\
 &\quad + (f_k(\mathbf{x}^k) - g_k(\mathbf{x}^k)) \tilde{\lambda}^\ell(\mathbf{x}^{k-1}) (f_k^{\ell-1}(\mathbf{x}^k))^T \\
 &\quad + (f_k(\mathbf{x}^k) - g_k(\mathbf{x}^k)) \tilde{\lambda}_k^\ell(\mathbf{x}^k) (f_k^{\ell-1}(\mathbf{x}^{k-1}))^T \Big) \\
 &\quad + \varepsilon^{2k} (f_k(\mathbf{x}^k) - g_k(\mathbf{x}^k)) \tilde{\lambda}_k^\ell(\mathbf{x}^k) (f_k^{\ell-1}(\mathbf{x}^k))^T,
 \end{aligned} \tag{116}$$

for all $k = 1 : m$.

Proof. By definition and the decomposition for $f(\mathbf{x}^k)$, $g(\mathbf{x}^k)$, $\tilde{\lambda}^\ell(\mathbf{x}^k)$, and $f_k^{\ell-1}(\mathbf{x}^k)$, we have

$$\begin{aligned}
 \left. \frac{\partial \mathcal{L}}{\partial W^\ell} \right|_{\mathcal{D}^k} &= \left\langle (f(\mathbf{x}^k) - g(\mathbf{x}^k)) \tilde{\lambda}^\ell(\mathbf{x}^k) (f_k^{\ell-1}(\mathbf{x}^k))^T \right\rangle_N \\
 &= \left\langle (f(\mathbf{x}^{k-1}) - g(\mathbf{x}^{k-1}) + \varepsilon^k (f_k(\mathbf{x}^k) - g_k(\mathbf{x}^{k-1}))) \right. \\
 &\quad \left. (\tilde{\lambda}^\ell(\mathbf{x}^{k-1}) + \varepsilon^k \tilde{\lambda}_k^\ell(\mathbf{x}^k)) (f_k^{\ell-1}(\mathbf{x}^{k-1}) + \varepsilon^k f_k^{\ell-1}(\mathbf{x}^k))^T \right\rangle_N \\
 &= \left\langle (f(\mathbf{x}^{k-1}) - g(\mathbf{x}^{k-1})) \tilde{\lambda}^\ell(\mathbf{x}^{k-1}) (f_k^{\ell-1}(\mathbf{x}^{k-1}))^T \right\rangle_N + \varepsilon^k \langle A_k^\ell(\mathbf{x}^k) \rangle_N \\
 &= \left. \frac{\partial \mathcal{L}(\theta)}{\partial W^\ell} \right|_{\mathcal{D}^{k-1}} + \varepsilon^k \langle A_k^\ell(\mathbf{x}^k) \rangle_N.
 \end{aligned} \tag{117}$$

□

Finally, we have the following main theorem about the multiscale structure of the gradient flow of DNNs.

Theorem B.14. For any DNN defined in Equation (6) and dataset under Assumption 2.1, we have

$$\frac{\partial \mathcal{L}(\theta)}{\partial W^\ell} = \sum_{k=0}^m \varepsilon^k \langle A_k^\ell(\mathbf{x}^k) \rangle_N, \tag{118}$$

where

$$A_0^\ell(\mathbf{x}^0) = (f(\mathbf{x}^0) - g(\mathbf{x}^0)) \tilde{\lambda}^\ell(\mathbf{x}^0) (f^{\ell-1}(\mathbf{x}^0))^T \tag{119}$$

and $\langle A_k^\ell(\mathbf{x}^k) \rangle_N$ follow the definitions in Equation (115) and Equation (116) in Lemma B.13 for $k = 1 : m$.

Proof. This is a direct result of applying Lemma B.13 repeatedly. □

We also want to point out that same structure of multiscale expansion occurs in other models: for linear regression, we have

$$\frac{d\theta}{dt} = \sum_{i=0}^d \varepsilon^i \langle A_i(\mathbf{x}^i) \rangle_N, \tag{120}$$

where

$$\langle A_i(\mathbf{x}^i) \rangle_N = \left\langle \mathbf{x}^i (\mathbf{x}^i)^T \right\rangle_N - \left\langle \mathbf{x}^{i-1} (\mathbf{x}^{i-1})^T \right\rangle_N, \tag{121}$$

with $\langle A_0(\mathbf{x}^0) \rangle_N = \left\langle \mathbf{x}^0 (\mathbf{x}^0)^T \right\rangle_N$.

For logistic regression, we still have

$$\frac{d\theta}{dt} = \sum_{i=0}^d \varepsilon^i \langle A_i(\mathbf{x}^i) \rangle_N. \tag{122}$$

C. Proof of multiscale gradient components and multiscale Hessian:

C.1. Multiscale gradient components in logistic regression

Proof. The label $g(\mathbf{x}_i) \in \mathbb{R}^k$ is a probability. Let $\mathbf{p}_i := g(\mathbf{x}_i)$, we have $\sum_{j=1}^k p_{ij} = 1$, and $p_{ij} > 0$. Then, the cross-entropy loss can be explicitly written as:

$$\mathcal{L}_c = -\frac{1}{N} \sum_{i=1}^N \mathbf{p}_i \cdot \log(\mathbf{f}(\mathbf{x}_i; \mathbf{w}, b)) = -\frac{1}{N} \sum_{i=1}^N \sum_{j=1}^k p_{ij} \log([f(\mathbf{x}_i; \mathbf{w}, b)]_j).$$

Recall that:

$$[f(\mathbf{x}; \mathbf{w}, b)]_j = \frac{e^{\mathbf{w}_j \cdot \mathbf{x} + b_j}}{\sum_{i=1}^k e^{\mathbf{w}_i \cdot \mathbf{x} + b_i}}, \quad j = 1 : k,$$

and note $\log(f_j) = (\mathbf{w}_j \cdot \mathbf{x} + b_j) - \log(\sum_i e_i)$, with $e_j := e^{\mathbf{w}_j \cdot \mathbf{x} + b_j}$, $f_j := [f(\mathbf{x}_i; \mathbf{w}, b)]_j$, for clarity. Therefore, for any weight \mathbf{w}_l :

$$\frac{\partial \log(f_j)}{\partial \mathbf{w}_l} = \left(\delta_{jl} - \frac{e_l}{\sum_i e_i} \right) \mathbf{x}^T$$

Then:

$$\frac{\partial \mathcal{L}_c}{\partial \mathbf{w}_l} = -\frac{1}{N} \sum_{i=1}^N \sum_{j=1}^k p_{ij} \left(\delta_{jl} - \frac{e_l}{\sum_i e_i} \right) \mathbf{x}_i^T = -\frac{1}{N} \sum_{i=1}^N \mathbf{x}_i^T \left(p_{il} - \frac{e_l}{\sum_i e_i} \right) = \langle (g(\mathbf{x})_l - f(\mathbf{x})_l) \mathbf{x}^T \rangle_N. \quad (123)$$

where the multiplier $(g(\mathbf{x}_i)_l - f(\mathbf{x}_i; \mathbf{w}, b)_l) \sim \mathcal{O}(1)$ in general. Therefore, it is straightforward to see that components in the loss gradient exhibits a similar multiscale behavior as the dataset, where the magnitude of the gradient aligns with the scale of the data distribution:

$$\frac{\partial \mathcal{L}_c}{\partial \mathbf{w}_l} \sim (\mathcal{O}(1), \mathcal{O}(\varepsilon_1), \mathcal{O}(\varepsilon_2) \dots). \quad (124)$$

Organizing the gradient for each \mathbf{w}_l into the matrix form leads us to the desired result. \square

C.2. Multiscale gradient components in neural network

Proof. The gradient of the loss concerning the first layer parameter W^1 is given by:

$$\frac{\partial \mathcal{L}}{\partial W^1} = \frac{1}{2N} \sum_{i=1}^N (f(\mathbf{x}_i, W) - g_i) \frac{\partial f}{\partial W^1},$$

where from the multiplicative representation:

$$\frac{\partial f}{\partial W^1} = \frac{\partial \tilde{f}}{\partial W^1} = \frac{\partial \tilde{f}(W^1 \mathbf{x}, W_2)}{\partial W^1 \mathbf{x}} \mathbf{x}^T.$$

Without loss of generality, we focus on the gradient of the first neuron, and let \mathbf{w}_{11} denote the first row of the weight matrix W^1 , such that $\mathbf{w}_{11} \cdot \mathbf{x}$ produces the first entry in the first hidden layer. Similarly, we have

$$\frac{\partial f}{\partial \mathbf{w}_{11}} = \frac{\partial \tilde{f}}{\partial \mathbf{w}_{11}} = \frac{\partial \tilde{f}(W^1 \mathbf{x}, W_2)}{\partial \mathbf{w}_{11}^T \mathbf{x}} \mathbf{x}^T.$$

Since f is a scalar function and $\mathbf{w}_{11}^T \mathbf{x}$ is also a scalar, we set $c_1 := \frac{\partial \tilde{f}(W^1 \mathbf{x}, W_2)}{\partial \mathbf{w}_{11}^T \mathbf{x}} \in \mathbb{R}$ for simplicity, which yields $\frac{\partial f}{\partial \mathbf{w}_{11}} = c_1 \mathbf{x}^T$, and the same applies for any row of the weight matrix W^1 . Let c_i denote the corresponding coefficient for the i -th row, and we have $\frac{\partial \tilde{f}}{\partial W^1} = \mathbf{c} \mathbf{x}^T$ where $\mathbf{c} = [c_1, c_2, \dots]^T$. Plug in the expression back to the loss gradient produces:

$$\frac{\partial \mathcal{L}}{\partial \mathbf{w}_{11}} = \frac{1}{2N} \sum_{i=1}^N (f(\mathbf{x}_i, W) - g_i) c_1(\mathbf{x}_i) \mathbf{x}_i^T. \quad (125)$$

The gradient expression in Equation (125) holds for any neuron in the first layer and closely matches with Equation (123). Thus, we can deduce that the gradient for W^1 also explicitly relies on the data distribution, where, if the data distribution satisfies Assumption 2.1, the gradient will have dimension-wise multiscale characteristics, akin to Equation (124). \square

C.3. Multiscale Hessian in neural network

Proof. Continued from Equation (125), to derive the Hessian we have:

$$\begin{aligned}\nabla_{\mathbf{w}_{11}}^2 \mathcal{L} &:= \frac{1}{2N} \sum_{i=1}^N \frac{\partial f(\mathbf{x}_i)}{\partial \mathbf{w}_{11}} c_1(\mathbf{x}_i) \mathbf{x}_i^T + (f(\mathbf{x}_i, W) - g_i) \nabla_{\mathbf{w}_{11}}^2 f(\mathbf{x}_i) \\ &= \frac{1}{2N} \sum_{i=1}^N c_1(\mathbf{x}_i)^2 \mathbf{x}_i \mathbf{x}_i^T + (f(\mathbf{x}_i, W) - g_i) \frac{\partial^2 \tilde{f}(W^1 \mathbf{x}_i, W_2)}{\partial (\mathbf{w}_{11}^T \mathbf{x}_i)^2} \mathbf{x}_i \mathbf{x}_i^T.\end{aligned}$$

Note that $(f(\mathbf{x}_i, W) - g_i), \frac{\partial^2 \tilde{f}(W^1 \mathbf{x}_i, W_2)}{\partial (\mathbf{w}_{11}^T \mathbf{x}_i)^2} \in \mathbb{R}$, setting:

$$s_j(\mathbf{x}_i) = c_j(\mathbf{x}_i)^2 + (f(\mathbf{x}_i, W) - g_i) \frac{\partial^2 \tilde{f}(W^1 \mathbf{x}_i, W_2)}{\partial (\mathbf{w}_{1j}^T \mathbf{x}_i)^2} \in \mathbb{R},$$

leads to

$$\nabla_{\mathbf{w}_{1j}}^2 \mathcal{L} = \frac{1}{2N} \sum_{i=1}^N s_j(\mathbf{x}_i) \mathbf{x}_i \mathbf{x}_i^T \approx \left(\sum_{i=1}^N s_j(\mathbf{x}_i) \right) X^T X,$$

which finishes the proof. \square

D. Proof of convergence properties of MrGD:

D.1. Proof of Theorem 3.4 (convergence for quadratic problems):

Lemma D.1. *For any $i = 2 : m$ and $j = 1 : m$, we have the following inequalities*

$$1 - R_i^j \kappa_i^{-1} \geq 1 - R_{i-1}^j \kappa_{i-1}^{-1} \quad (126)$$

Proof. Direct calculation gives:

$$1 - R_i^j \kappa_i^{-1} = 1 - \eta_j \sigma_i \frac{\sigma_{i,d_i}}{\sigma_i} = 1 - \eta_j \sigma_{i,d_i} \geq 1 - \eta_j \sigma_{i-1,d_{i-1}} = 1 - R_{i-1}^j \kappa_{i-1}^{-1}$$

\square

The Main Proof:

Proof. Let V_i be the eigenspace corresponding to the i -th group eigenvalues of A , and we can write:

$$\mathbb{R}^d = V = V_1 \oplus V_2 \oplus \cdots \oplus V_m, \quad (127)$$

since A is symmetric and different groups of eigenvalues are distinct. This decomposition leads to

$$\|S\| = \sup_{\|v\|=1} \|Sv\| \leq \max_{i=1:m} \sup_{v_i \in V_i, \|v_i\|=1} \|Sv_i\| \quad (128)$$

since S is a polynomial of A and $\{V_i\}_{i=1}^m$ are also the eigenspaces of S , orthogonal to each other.

Then, the proof idea can be divided into two steps. First, we establish that for any $i = 1 : m$, there exists some constant c_i 's such that

$$\sup_{v_i \in V_i, \|v_i\|=1} \|Sv_i\| \leq c_i. \quad (129)$$

Subsequently, we demonstrate that by posing suitable conditions on n_i 's, these c_i 's satisfy:

$$c_{i+1} \geq c_i, \quad \forall i = 1 : m - 1. \quad (130)$$

Consequently, if we finish the aforementioned two steps, we can conclude that

$$\|S\| \leq c_m,$$

Step 1: Following the discussion from Remark 3.2, c_i 's in Equation (129) can be chosen as:

$$\sup_{v_i \in V_i, \|v_i\|=1} \|Sv_i\| \leq c_i := \prod_{j=1}^i (1 - R_i^j \kappa_i^{-1})^{n_j} \prod_{j=i+1}^m |1 - R_i^j|^{n_j}. \quad (131)$$

In particular, we have

$$\sup_{v_m \in V_m, \|v_m\|=1} \|Sv_m\| = \prod_{j=1}^m (1 - R_m^j \kappa_m^{-1})^{n_j} =: c_m. \quad (132)$$

Step 2: We derive sufficient conditions for Equation (130) by induction from $m - 1$ to 1. This process will generate conditions on n_i 's along the way.

For $i = m - 1$, we want to ensure $c_m \geq c_{m-1}$, that is:

$$\prod_{j=1}^m (1 - R_m^j \kappa_m^{-1})^{n_j} \geq \prod_{j=1}^{m-1} (1 - R_{m-1}^j \kappa_{m-1}^{-1})^{n_j} |1 - R_{m-1}^m|^{n_m}.$$

We divide the above into two parts, where the first part is to consider only up to $j = m - 2$, and is directly given by Lemma D.1:

$$\prod_{j=1}^{m-2} (1 - R_m^j \kappa_m^{-1})^{n_j} \geq \prod_{j=1}^{m-2} (1 - R_{m-1}^j \kappa_{m-1}^{-1})^{n_j}, \quad (133)$$

for arbitrary $n_j > 0$. Thereby, we only need to ensure that the second part holds:

$$(1 - R_m^{m-1} \kappa_m^{-1})^{n_{m-1}} (1 - R_m^m \kappa_m^{-1})^{n_m} \geq (1 - R_{m-1}^{m-1} \kappa_{m-1}^{-1})^{n_{m-1}} |1 - R_{m-1}^m|^{n_m}.$$

A direct calculation yields:

$$n_{m-1} \log \left(\frac{1 - R_m^{m-1} \kappa_m^{-1}}{1 - R_{m-1}^{m-1} \kappa_{m-1}^{-1}} \right) \geq n_m \log \left(\frac{|1 - R_{m-1}^m|}{1 - R_m^m \kappa_m^{-1}} \right).$$

By setting:

$$F_{m-1,m} = \left(-\log(r_{m-1}) + \log \left(\frac{|r_{m-1} - R_m^m|}{1 - R_m^m \kappa_m^{-1}} \right) \right) / \log \left(\frac{1 - R_m^{m-1} \kappa_m^{-1}}{1 - R_m^m \kappa_m^{-1}} \right),$$

we obtain the following sufficient condition for $c_m \geq c_{m-1}$:

$$n_{m-1} \geq n_m F_{m-1,m}. \quad (134)$$

Inductively, assume $n_{m-1}, n_{m-2}, \dots, n_{i+1}$ have been properly defined such that $c_{j+1} \geq c_j$ holds for all $j = i + 1 : m - 1$, we aim to derive a condition on n_i as the sufficient condition for

$$c_{i+1} \geq c_i. \quad (135)$$

We again divide Equation (135) into two parts, and invoke Lemma D.1 for the first part up to $j = i - 1$:

$$\prod_{j=1}^{i-1} (1 - R_{i+1}^j \kappa_{i+1}^{-1})^{n_j} \geq \prod_{j=1}^{i-1} (1 - R_i^j \kappa_i^{-1})^{n_j}, \quad (136)$$

for arbitrary $n_j > 0$. The second part needs to satisfy:

$$\begin{aligned} & (1 - R_{i+1}^i \kappa_{i+1}^{-1})^{n_i} (1 - R_{i+1}^{i+1} \kappa_{i+1}^{-1})^{n_{i+1}} \prod_{j=i+2}^m |1 - R_{i+1}^j|^{n_j} \\ & \geq (1 - R_i^i \kappa_i^{-1})^{n_i} |1 - R_i^{i+1}|^{n_{i+1}} \prod_{j=i+2}^m |1 - R_i^j|^{n_j}. \end{aligned} \quad (137)$$

We claim the following condition on n_i is sufficient for the purpose,

$$n_i \geq \left\lceil \sum_{j=i+1}^m n_j F_{i,j} \right\rceil, \quad (138)$$

where $F_{i,j}$ will be determined shortly. Thus, we only need to check Equation (137) by setting $n_i = \sum_{j=i+1}^m n_j F_{i,j}$ whereby the equation can be further divided into two separate parts:

$$(1 - R_{i+1}^i \kappa_{i+1}^{-1})^{n_{i+1} F_{i,i+1}} (1 - R_{i+1}^{i+1} \kappa_{i+1}^{-1})^{n_{i+1}} \geq (1 - R_i^i \kappa_i^{-1})^{n_{i+1} F_{i,i+1}} |1 - R_i^{i+1}|^{n_{i+1}}, \quad (139)$$

and

$$(1 - R_{i+1}^i \kappa_{i+1}^{-1})^{n_j F_{i,j}} |1 - R_{i+1}^j|^{n_j} \geq (1 - R_i^i \kappa_i^{-1})^{n_j F_{i,j}} |1 - R_i^j|^{n_j}, \quad (140)$$

for all $j = i + 2 : m$. Similarly, a direct calculation gives:

$$F_{i,i+1} = \left(-\log(r_i) + \log \left(\frac{|r_i - R_{i+1}^{i+1}|}{1 - R_{i+1}^{i+1} \kappa_{i+1}^{-1}} \right) \right) / \log \left(\frac{1 - R_{i+1}^i \kappa_{i+1}^{-1}}{1 - R_i^i \kappa_i^{-1}} \right),$$

and

$$F_{i,j} = \left(-\log(r_i) + \log \left(\frac{|r_i - R_{i+1}^j|}{1 - R_{i+1}^j \kappa_{i+1}^{-1}} \right) \right) / \log \left(\frac{1 - R_{i+1}^i \kappa_{i+1}^{-1}}{1 - R_i^i \kappa_i^{-1}} \right),$$

for all $j = i + 2 : m$. □

D.2. Proof for Corollary 3.9

Proof. First, we notice that the denominators of $F_{i,i+1}$ and $F_{i,j}$ for $j = i + 2 : m$ given by Theorem 3.4 are the same and larger than 0. Therefore, we first give a lower bound on the denominator:

$$\begin{aligned} \log \left(\frac{1 - R_{i+1}^i \kappa_{i+1}^{-1}}{1 - R_i^i \kappa_i^{-1}} \right) &= \log \left(\frac{1 - \eta_i \sigma_{i+1, d_{i+1}}}{1 - \eta_i \sigma_{i, d_i}} \right) = \log \left(\frac{1 - \frac{r}{\eta \kappa_c}}{1 - \frac{1}{\eta \kappa_c}} \right) \\ &= \log \left(1 - \frac{r}{\eta \kappa_c} \right) - \log \left(1 - \frac{1}{\eta \kappa_c} \right). \end{aligned}$$

Recall the log-inequality:

$$1 - \frac{1}{x} \leq \log(x) \leq x - 1 \text{ for } x > 0, \quad \implies \quad \frac{-x}{1-x} \leq \log(1-x) \leq -x \text{ for } x < 1.$$

Since $\eta \kappa_c > 1$ and $r < 1$, the log-inequality yields the following bound on the denominator:

$$\log \left(\frac{1 - R_{i+1}^i \kappa_{i+1}^{-1}}{1 - R_i^i \kappa_i^{-1}} \right) \geq \frac{-\frac{r}{\eta \kappa_c}}{1 - \frac{r}{\eta \kappa_c}} + \frac{1}{\eta \kappa_c} = \frac{\eta \kappa_c (1-r) - r}{\eta \kappa_c (\eta \kappa_c - r)}.$$

As for the numerator for $F_{i,i+1}$, since $r_i = r \ll 1$, it satisfies:

$$\left(-\log(r_i) + \log \left(\frac{|r_i - R_{i+1}^{i+1}|}{1 - R_{i+1}^{i+1} \kappa_{i+1}^{-1}} \right) \right) \geq \log \left(\frac{|1 - \eta_{i+1} \sigma_i|}{1 - \eta_{i+1} \sigma_{i+1, d_{i+1}}} \right) > 0.$$

Hence, we derive a corresponding upper bound:

$$\begin{aligned} \log\left(\frac{|1 - \eta_{i+1}\sigma_i|}{1 - \eta_{i+1}\sigma_{i+1,d_{i+1}}}\right) &= \log\left(\frac{\kappa_c - \eta\kappa_c r}{\eta\kappa_c r - r}\right) = \log(\kappa_c) + \log(1 - \eta r) - \log(r) - \log(\eta\kappa_c - 1) \\ &\leq -\log(r) - \log(\eta\kappa_c - 1) + \kappa_c - \eta r - 1. \end{aligned}$$

Next, for $F_{i,j}$ with $j = i + 2 : m$, we denote $k = j - (i + 1) \geq 1$ and its numerator becomes:

$$\left(-\log(r_i) + \log\left(\frac{|r_i - R_{i+1}^j|}{|1 - R_{i+1}^j|}\right)\right) = -\log(r) + \log\left(\frac{1 - \eta r^{k+1}}{1 - \eta r^k}\right) \geq 0,$$

since $r \ll 1$. Again, we derive a corresponding upper bound by applying the log-inequality:

$$\log\left(\frac{1 - \eta r^{k+1}}{1 - \eta r^k}\right) = \log(1 - \eta r^{k+1}) - \log(1 - \eta r^k) \leq -\eta r^{k+1} + \frac{\eta r^k}{1 - \eta r^k} \sim o(r^k).$$

Therefore, there is a constant $C > 0$ (depends on k, ε , and η) s.t. the numerator is bounded above:

$$\log\left(\frac{1 - \eta r^{k+1}}{1 - \eta r^k}\right) \leq C r^k, \quad (141)$$

for any $r \in (0, \varepsilon)$. This finishes the proof. \square

D.3. Proof of Theorem 3.12 (convergence for convex problems):

Proof. First, by the fundamental Theorem of calculus, we have the following identity

$$\nabla\mathcal{L}(\theta) = \nabla\mathcal{L}(\theta) - \nabla\mathcal{L}(\theta^*) = \mathcal{H}_\theta(\theta - \theta^*),$$

where $\mathcal{H}_\theta \in \mathbb{R}^{d \times d}$ is obtained by integrating $\nabla^2\mathcal{L}$ along the path from θ^* to θ . More precisely, we have

$$\mathcal{H}_\theta = \int_{t=0}^1 \nabla^2\mathcal{L}(\theta_t) dt,$$

where $\theta_t = t\theta + (1-t)\theta^*$. Given Assumption 3.10 for $\nabla^2\mathcal{L}(\theta)$, using the triangle inequality for integral, we can deduce that \mathcal{H}_θ also satisfies Assumption 3.10 for any θ . As a result,

$$\theta_{j,s+1}^k - \theta^* = \theta_{j,s}^k - \theta^* - \eta_j \nabla\mathcal{L}(\theta_{j,s}^k) = (\mathbf{I}_d - \eta_j \mathcal{H}_{j,s}^k)(\theta_{j,s}^k - \theta^*). \quad (142)$$

The idea of the remaining proof is to decompose the error term into different orthogonal spaces, and show the error will be bounded on each of the space. To this end, let us denote the component of the error in the i -th space by

$$v_i^{j,s} := \Pi_i(\theta_{j,s}^k - \theta^*),$$

where Π_i is the row-orthogonal matrix defined in Equation (29). Then, we apply Π_i to Equation (142) to get the error in the i -th space for the next step, we obtain

$$\begin{aligned} \|v_i^{j,s+1}\| &= \left\| \Pi_i(\mathbf{I}_d - \eta_j \mathcal{H}_{j,s}^k) \left(\sum_{\ell=1}^m \Pi_\ell^T v_\ell^{j,s} \right) \right\| \\ &\leq \left\| (\mathbf{I}_{d_i} - \eta_j \Pi_i \mathcal{H}_{j,s}^k \Pi_i^T) v_i^{j,s} \right\| + \sum_{\ell \neq i} \eta_j \left\| \Pi_i \mathcal{H}_{j,s}^k \Pi_\ell^T v_\ell^{j,s} \right\| \\ &\leq \left\| (\mathbf{I}_{d_i} - \eta_j \Pi_i \mathcal{H}_{j,s}^k \Pi_i^T) \right\| \|v_i^{j,s}\| + \delta \eta_j \sum_{\ell \neq i} \left\| \Pi_\ell(\theta_{j,s}^k - \theta^*) \right\| \\ &\leq \left\| (\mathbf{I}_{d_i} - \eta_j \Pi_i \mathcal{H}_{j,s}^k \Pi_i^T) \right\| \|v_i^{j,s}\| + \delta \eta_j \|\theta_{j,s}^k - \theta^*\| \\ &\leq \begin{cases} (1 - R_i^j \kappa_i^{-1}) \|v_i^{j,s}\| + \delta \eta_j C & \text{if } j \leq i, \\ |1 - R_i^j| \|v_i^{j,s}\| + \delta \eta_j C & \text{if } j > i. \end{cases} \end{aligned} \quad (143)$$

By repeating the above process from v_i^{j,n_j} to $v_i^{j,0}$, we have

$$\begin{aligned} \|v_i^{j,n_j}\| &\leq \begin{cases} \left(1 - R_i^j \kappa_i^{-1}\right)^{n_j} \|v_i^{j,0}\| + \delta \eta_j C E_i^j & \text{if } j \leq i, \\ |1 - R_i^j|^{n_j} \|v_i^{j,0}\| + \delta \eta_j C E_i^j & \text{if } j > i, \end{cases} \\ &= \begin{cases} \left(1 - R_i^j \kappa_i^{-1}\right)^{n_j} \|v_i^{j+1,n_{j+1}}\| + \delta \eta_j C E_i^j & \text{if } j \leq i, \\ |1 - R_i^j|^{n_j} \|v_i^{j+1,n_{j+1}}\| + \delta \eta_j C E_i^j & \text{if } j > i. \end{cases} \end{aligned} \quad (144)$$

since $\theta_{j,0}^k = \theta_{j+1,n_{j+1}}^k$, where

$$E_i^j = \begin{cases} \sum_{s=0}^{n_j-1} \left(1 - R_i^j \kappa_i^{-1}\right)^s & \text{if } j \leq i, \\ \sum_{s=0}^{n_j-1} |1 - R_i^j|^s & \text{if } j > i. \end{cases} \quad (145)$$

By re-applying the inequality in Equation (144) repeatedly on $\|v_i^{1,n_1}\|$ we have

$$\|v_i^{1,n_1}\| \leq c_i \|v_i^{m,0}\| + \delta C \sum_{j=0}^{m-1} \eta_{j+1} C_i^j E_i^j, \quad (146)$$

where

$$c_i = \prod_{j=1}^i \left(1 - R_i^j \kappa_i^{-1}\right)^{n_j} \prod_{j=i+1}^m |1 - R_i^j|^{n_j}, \quad (147)$$

matched with the definition given in Equation (131) for all $i = 1 : m$ and

$$C_i^j = \begin{cases} \prod_{s=1}^j \left(1 - R_i^s \kappa_i^{-1}\right)^{n_s} & \text{if } j \leq i, \\ \prod_{s=1}^i \left(1 - R_i^s \kappa_i^{-1}\right)^{n_s} \prod_{s=i+1}^j |1 - R_i^s|^{n_s} & \text{if } j > i. \end{cases} \quad (148)$$

Adopting the notation $\theta^k = \theta_{1,n_1}^k$, for a fixed k , we have:

$$\begin{aligned} \|\theta^k - \theta^*\| &= \sum_{i=1}^m \|\Pi_i(\theta^k - \theta^*)\| = \sum_{i=1}^m \|v_i^{1,n_1}\| \\ &\leq \sum_{i=1}^m c_i \|v_i^{m,0}\| + \delta C \sum_{i=1}^m 1 \times \sum_{j=0}^{m-1} C_i^j E_i^j \\ &\leq \max_{i=1:m} \{c_i\} \sum_{i=1}^m \|v_i^{m,0}\| + \delta m C \max_{i=1:m} \left\{ \sum_{j=0}^{m-1} C_i^j E_i^j \right\} \\ &= \max_{i=1:m} \{c_i\} \|\theta^{k-1} - \theta^*\| + \delta m C \max_{i=1:m} \left\{ \sum_{j=0}^{m-1} C_i^j E_i^j \right\} \end{aligned} \quad (149)$$

since $\theta_{m,0}^k = \theta^{k-1}$. Recalling Equation (130) in the proof of Theorem 3.4 in Appendix D.1, we have

$$\max_{i=1:m} \{c_i\} = c_m = \prod_{j=1}^m \left(1 - R_m^j \kappa_m^{-1}\right)^{n_j}, \quad (150)$$

if n_{m-1}, \dots, n_2, n_1 satisfy the condition in Equation (18). This finishes the proof for Theorem 3.11. \square

E. Numerical example for linear regression with multiscale data

First, the linear regression problem depicted in Figure 3 is represented as

$$\min_w \frac{1}{N} \sum_{i=1}^N (w \cdot \mathbf{x}_i - g_i)^2 \Leftrightarrow Aw = b,$$

where $A = \frac{1}{N} \sum_{i=1}^N \mathbf{x}_i \mathbf{x}_i^T \in \mathbb{R}^{100 \times 100}$ and $b = \frac{2}{N} \sum_{i=1}^N g_i \mathbf{x}_i \in \mathbb{R}^{100}$. In the numerical results presented in Figure 3, we record the residual $\|Aw^k - b\|$ on the vertical axis. For the GD method, k represents the number of GD steps. For MrGD, k denotes the total number of iterations, i.e., including both inner and outer iterations.

Two-Scale Problems. We sample the data $\mathbf{x}_i = (\mathbf{x}_i^0, \sqrt{\varepsilon} \mathbf{x}_i^1) \in \mathbb{R}^{d_0+d_1}$, where $d_0 = 80$ and $d_1 = 20$. Specifically, we set $\varepsilon = 0.001$, sample $g_i \sim N(0, 1)$, and sample $\mathbf{x}_i^k \sim N(0, I_{d_k})$ for $k = 0, 1$ and $i = 1 : N$ with $N = 10^4$. For this case, we can approximately have that $r \approx \varepsilon = 0.001$ and the global condition number of A is around r^{-1} . In the MrGD algorithm, we set $\eta_0 = 0.5$, $\eta_1 = \frac{1}{2r}$, and $n_1 = 15$.

Three-Scale Problems. We sample the data $\mathbf{x}_i = (\mathbf{x}_i^0, \sqrt{\varepsilon} \mathbf{x}_i^1, \varepsilon \mathbf{x}_i^2) \in \mathbb{R}^{d_0+d_1+d_2}$, where $d_0 = 60$, $d_1 = 20$, and $d_2 = 20$. Specifically, we set $\varepsilon = 0.1$, sample $g_i \sim N(0, 1)$, and sample $\mathbf{x}_i^k \sim N(0, I_{d_k})$ for $k = 0, 1, 2$ and $i = 1 : N$ with $N = 10^4$. For this case, we can approximately have that $r \approx \varepsilon = 0.1$ and the global condition number of A is around r^{-2} . In the MrGD algorithm, we set $\eta_0 = 0.5$, $\eta_1 = \frac{1}{2r}$, and $\eta_2 = \frac{1}{2r^2}$ with $n_1 = 3$ and $n_2 = 15$.

F. CIFAR MNIST Comparison

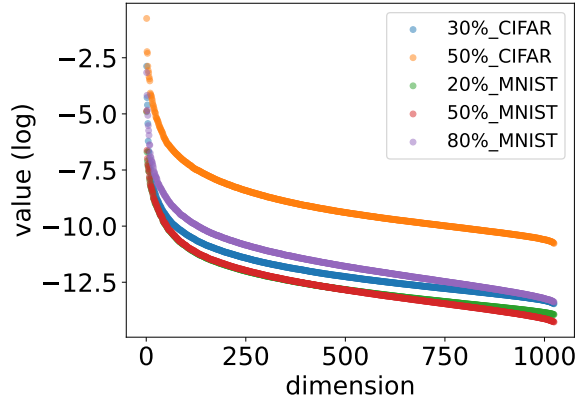


Figure 4. Comparison of eigenvalues (sorted by magnitudes) of the Hessian in the second hidden layer, under the natural log scale. The CIFAR models are those from Section 2.2. The MNIST model is also a 3-layer MLP of sizes 784-1024-128-10, identical to the CIFAR model except for the input dimension. The MNIST model is also trained under the same setting: full gradient descent, fixed learning rate 0.1, and cross-entropy loss. Three stages in training of the MNIST model with test accuracy 20%, 50%, and 80%, respectively are presented. All models in both the CIFAR and MNIST exhibit similar decaying property.